ADDIS ABABA UNIVERSITY

SCHOOL OF GRADUATE STUDIES

ADDIS ABABA INSTITUTE OF TECHNOLOGY

ELECTRICAL AND COMPUTER ENGINEERING

Study and Review on the Design and Performance Aspects of III-V Semiconductor Solar Cells

(Case Study: Comparison on GaAs, Ge, and Si substrate)

By

Netsanet Behailu

Advisor

Professor Mohammed Abdo

A Thesis Submitted to the School of Graduate Studies of Addis Ababa University in Partial Fulfillment of the Requirements for the Degree of Masters of Science in Microelectronics Engineering

November 2016

Addis Ababa, Ethiopia

ADDIS ABABA UNIVERSITY

SCHOOL OF GRADUATE STUDIES

ADDIS ABABA INSTITUTE OF TECHNOLOGY

ELECTRICAL AND COMPUTER ENGINEERING

Study and Review on the Design and Performance Aspects of III-V Semiconductor Solar Cells

(Case Study: Comparison on GaAs, Ge and Si substrate)

By

Netsanet Behailu

ADDIS ABABA INSTITUTE OF TECHNOLOGY APPROVED BY BOARD OF EXAMINERS

Chairman (Department of Graduate Committee)	Signature
Advisor	Signature
Internal Examiner	Signature
External Examiner	Signature

Abstract

This thesis focuses on studying and reviewing the design and performance aspects of III-V Solar cells; and make a comparison among the solar cells on GaAs, Ge, and Si substrate mainly based on efficiency and cost. The performances of 1-junction GaAs and 2-junction InGaP/GaAs solar cells on GaAs substrate is reviewed and the latest efficiencies are found to be 28.8% and 34.1% respectively. The performance of 3-Junction solar cell on Ge substrate is also reviewed and the latest efficiency is 44.4%. Finally, the performance of 1-Junction, 2-Junction and 3-Junction III-V solar cells on Si substrate is reviewed and the recent efficiencies are 26%, 29.2% and 33.5% respectively. Regarding the cost, one of the most significant cost contributors for III-V solar cells is the cost of the starting substrate. A recent study has revealed that transitioning of a 4” Ge or GaAs substrate to 8” Si substrate would correlate to about 60% reduction in cost for multijunction solar cells.

In general, the review shows that the efficiencies of III-V solar cells on Si substrate are continually increasing and recently, the efficiencies of 1-Junction and 2-Junction III-V solar cells on Si substrate become comparable to the one on GaAs substrate. The study indicates that the successful integration of III-V solar cells on Si substrate offers a great promise for lowering the cost of solar energy by combining the high efficiency merits of the III-V materials with the low-cost and abundance of the Si substrate.

Acknowledgment

I would like to sincerely thank my adviser, Professor Mohammed Abdo for giving me a chance to perform the research work under his supervision. I am grateful to him for his continual review and support. I would like also to thank Dr. Getachew Alemu and Dr. Berhanu Bulcha for their support during my research work and for being excellent mentors.

The Microelectronics Engineering learning process was challenging and worthwhile. I would like to thank all my teachers and friends who have assisted me during the last three years. I would like to forward my special thanks to my family for their love and support. Above all, I praise God for helping me and giving me the strength to finalize the Masters course work and Thesis.

TABLE OF CONTENTS

List of Figures

List of Tables

List of Acronyms

AM	Air Mass
AM0	Air Mass 0
AM1.5d	Air Mass 1.5 Direct
AM1.5g	Air Mass 1.5 Global
ARC	Anti Reflective Coating
BSF	Back Surface Field
CVD	Chemical Vapor Deposition
FF	Fill Factor
IC	Integrated Circuit
IQE	Internal Quantum efficiency
LEC	Liquid Encapsulated Czochralski
LPE	Liquid Phase Epitaxy
MBE	Molecular Beam Epitaxy
MEMS	Micro Electromechanical System
MOCVD	Metal Organic Chemical Vapor Deposition
MOVPE	Metal Organic Vapor Phase Epitaxy
NREL	National Renewable Energy Laboratory
p-n	Positive negative
PV	Photovoltaic
QE	Quantum efficiency
QFL	Quasi Fermi Level
SCR	Space Charge Region
SRH	Shockley Reed Haul
TDD	Threading Dislocation Density
VPE	Vapor Phase Epitaxy
3D	3 Dimensional

List of Symbols

Å	Angstrom
$b_s(E)$	Incident photon flux density
D_n or D_p	Minority carrier diffusion coefficient
E_F	Fermi Level
E_{Fn}, E_{Fp}	Minority electron/hole quasi-Fermi level
GaAs	Gallium Arsenide
Ge	Germanium
III-V	Group 3 and 5 Semiconductor Compound
InGaP	Indium Gallium Phosphide
J_{dark}	Dark current
J_o	Diode saturation current density
J_m	Current density at the maximum power point
J_{ph}	Photo generated current density
J_{RAD}	Current density corresponding to the emitted luminescent flux at bias V
J_{sc}	Short-circuit current density
K	Boltzmann Constant
n	Diode ideality factor
n_{ip}, n_{in}	Intrinsic Carrier Concentration
P_m	Maximum power point
q	Charge
R_s, R_{sh}	Series resistance, Shunt resistance
Si	Silicon
S_n, S_p	Surface recombination Velocity
$\tau_n$or τ_p	Minority carrier lifetime
V_m	Voltage at the maximum power point
V_{oc}	Open circuit voltage
W_D	Depletion Width
Z	Zenith Angle
λ	Wavelength
η	Efficiency of a solar cell

CHAPTER 1

INTRODUCTION

Among Ethiopia's 90 million populations, 85% live in rural areas[1] and most of them still have no access to electricity. The low demand and sparse population distribution makes it very expensive to reach these areas through grid extension. Hence, off grid power supply is an alternative source for rural electrification.

Photovoltaic is recognized as an important off-grid power source[2] since it uses inexhaustible solar energy, has a rapid response, can operate at moderate temperatures, and produces no pollution while producing electricity.

Edmund Becquerel is the first physicist who observed the photovoltaic effect; conversion of light to electricity; in 1839[2]. Becquerel observed voltage during illumination of electrodes in a weak conducting solution. The Photovoltaic effect was first studied in solids, such as selenium, in the 1870s. Selenium photovoltaic cells with conversion efficiency of 1-2% were built in the 1880s[3]. However, Selenium cell was not applied as energy converter due to its high cost and very low efficiency. In the 1920s and 1930s, quantum mechanics laid the theoretical base for the present Photovoltaic technology. Bell Telephone Laboratory achieved 4% efficiency with silicon photovoltaic cell in 1954 and soon enhanced the efficiency to 6% and 11%[3], indicating new era of power-producing cells.

In 1950s, silicon PV cells were tried to be commercialized to the regions that were geographically isolated from electric grid. But, in 1958, a small PV cell (less than one-watt) was used by U.S. Vanguard space satellite to power the radio[4]. The cells performed effectively and the space scientists recognized the PV cell as a good power source for space missions. Technology development of the solar cell has been a part of the space program ever since[2].

The most common materials for solar cell applications are based on silicon, and GaAs. These solar cells have efficiencies more than 15%[12]. Organic solar cells are introduced recently but, are not well commercialized yet due to their low efficiency[5]. Silicon cells lead the terrestrial solar cell market because of their relatively lower cost.

The III-V compound semiconductor solar cells have exhibited high-efficiency. However, their expensive cost has limited their application for terrestrial sector and are mainly used for the space and satellite applications. The III-V compound semiconductor based 3-junction solar cells currently hold the world record efficiency of 44%[5] under concentrated sunlight of 947 suns.

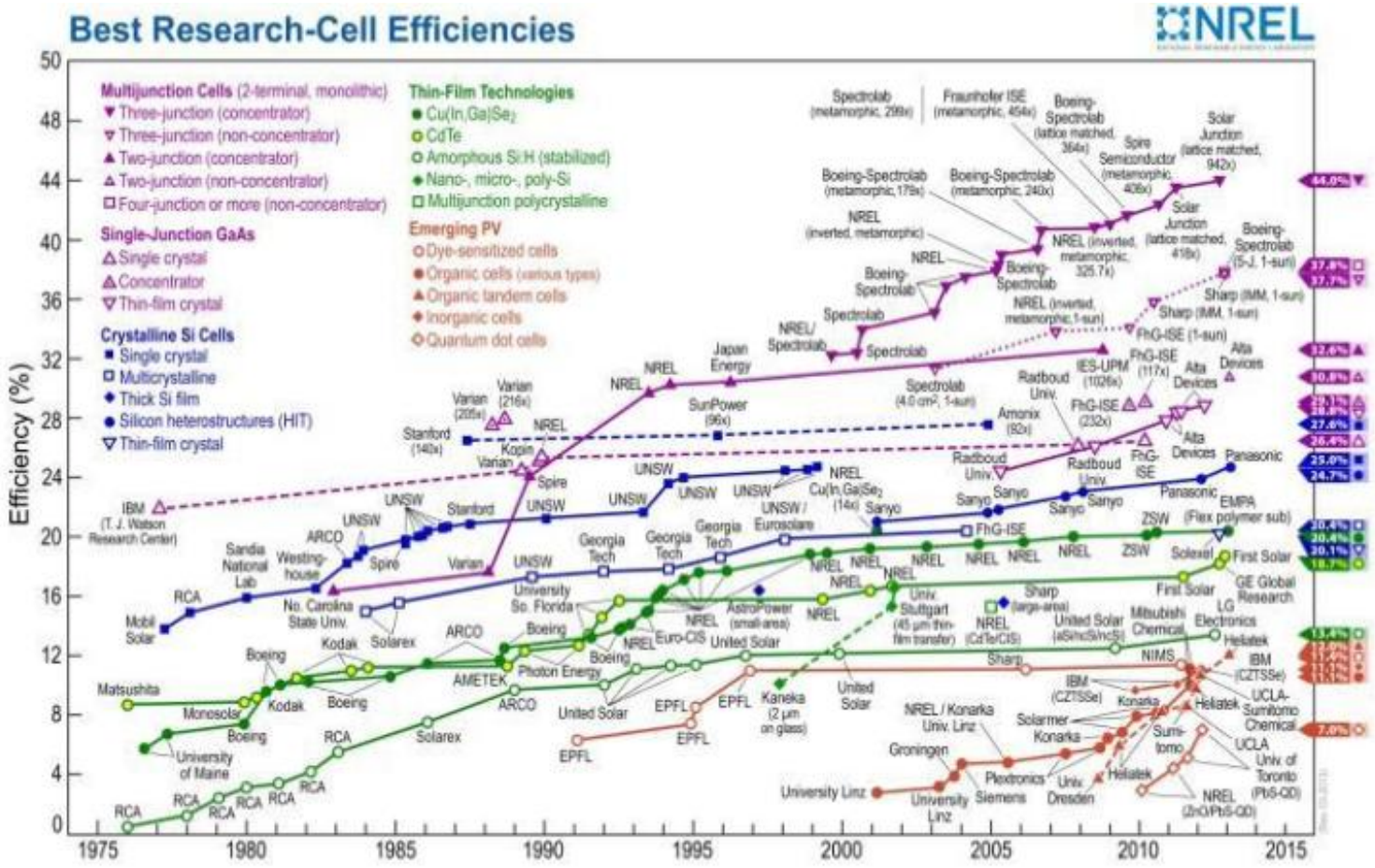

Figure 1.1 Progress in various solar cell technologies over the last 40 years[6].

The U.S. Department of Energy's National Renewable Energy Laboratory has plotted in a single graph the progress made by various solar technologies in the last 40 years as shown in Figure 1.1[6].

1.1 Research Objective

General Objective

The general objective of this thesis is to study and review the design and performance aspects of III-V semiconductor solar cells.

Specific Objective

- Compare III-V Solar Cell on GaAs, Ge and Si substrate.
- Evaluate the performance of III-V Solar cells based on efficiency and cost.
- Suggest the best option for high efficiency and low cost III-V solar cells.

1.2 Research Methodology

Quantitative method is used for this work. The III-V compound semiconductor multijunction solar cells have high conversion efficiency but their expensive cost has limited their applications. A quantitative method is used to realize the conversion efficiency and cost of multijunction III-V solar cells on different substrates and to make comparison and recommendation for the best option of high efficiency and low cost solar cells.

Data on III-V semiconductor solar cell performances were collected from Publications, Articles, Thesis papers, Solar Efficiency Table, and National Renewable Energy Laboratory Website.

First, multi-Junction III-V Solar Cells on GaAs and Ge substrate were analyzed. The conversion efficiencies of these solar cells are continually increasing but their high cost has limited the applicability for terrestrial sector. Following that, the performances of multijunction III-V Solar cells on Si substrate were assessed. The efficiencies of 1-Junction and 2-Junction Solar cells on Si substrate were comparable to the one on GaAs substrate. But, more work is required to get comparable result for 3-Junction solar cells on Si substrate with the one on Ge substrate. Si is abundantly available and cheaper than GaAs and Ge. So, integrating the III-V solar cells on Si substrate is very promising to have high efficiency and low cost solar cells.

1.3 Organization of This Thesis

In Chapter 2, the solar spectrum and operation of solar cells is discussed along with characteristics and structure of solar cells. The basics of III-V solar cells, types of III-V solar cells substrates and the design fundamentals are presented in Chapter 3. Chapter 4 describes 1-junction, 2-junction and 3-junction III-V solar cells on GaAs, Ge and Si substrate. In Chapter 4, short circuit current (I_{sc}), open circuit voltage (V_{oc}), fill factor (FF), efficiency (η) and cost are used to make a comparison among III-V solar cells on different substrates. Finally, the performance of III-V solar cells on different substrates is discussed. The results of the review provide a quantitative assessment of III-V solar cell figure-of-merits as a function of different substrates. Chapter 5 concludes the thesis, the results are summarized and recommendation for the future works are also presented.

CHAPTER 2

SOLAR CELLS

2.1 Solar Spectrum

The solar spectrum and the related solar intensity that reaches the earth's surface are different from the spectrum that reaches the outer space; the air mass coefficients (AM) is defined to make a comparison. Air mass defines the path length of radiation through the atmosphere in relation to the shortest length if the sun was in the apex[7]. The air mass coefficient for solar radiations incident at a zenith angle (z) relative to the normal to the earth's surface is defined as:

$$AM = \frac{1}{\cos(Z)} \qquad (2.1)$$

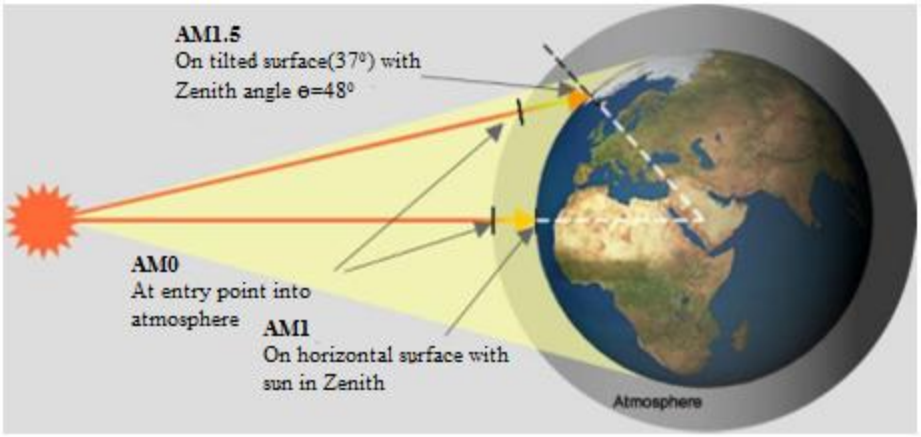

Figure 2.1 Illustration of various air mass (AM) position and the zenith point [7].

Figure 2.1 shows the solar radiation at different locations; AM0 is the radiation before entering to the earth surface, AM1 is the radiation on horizontal earth surface with sun in zenith and AM1.5 is the radiation on the tilted surface with zenith angle of 48^0[7]. AM1.5 is the standard coefficient used to represent the solar radiation in the earth surface.

The standard air masses for space, terrestrial and concentrated sunlight are defined as AM0, AM1.5G (global) and AM1.5D (direct), respectively and the corresponding spectrums are shown in Fig 2.2[6]. The corresponding incident intensities for AM0, AM1.5G and AM1.5D are ~1356 W/m^2, ~1000 W/m^2 and ~887 W/m^2 respectively.

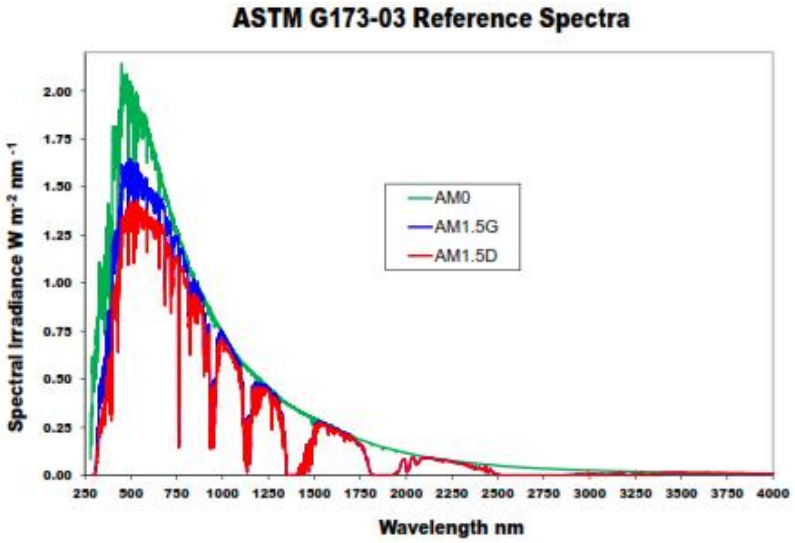

Figure 2.2 Solar Spectrum for AM0, AM1.5G, AM1.5D[6].

Figure 2.3 shows the terrestrial solar radiations which are, Direct and Global radiations[8]. The direct radiation represents the radiation directly from the sun; and the global radiation represents the direct radiation plus the diffused radiation.

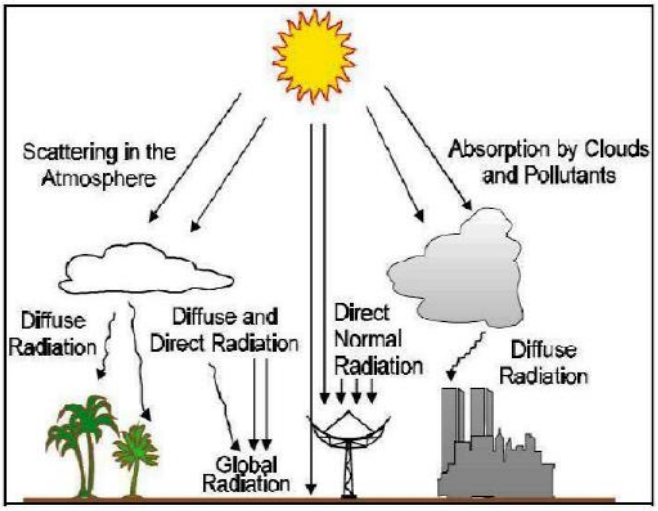

Figure 2.3 overview of terrestrial solar radiation[8].

2.2 Solar Cell Operation

In a solar cell, if the incident photon energy is greater than the band-gap energy of the cell, it will be absorbed and electron will be excited from the valence band to the conduction band to create an electron-hole pair[9]. These generated carriers will diffuse through the quasi-neutral region and drift to the p-n junction due to the built-in electric field. Electrons generated in the p-side travel towards the n-side and holes generated in the n-side travel towards the p-side[10]. Potential difference occurs due to the distribution of carriers; the split of the thermal equilibrium Ferm-level (E_F) into minority electron quasi-Fermi level (E_{Fn}), and minority hole quasi-Fermi level, E_{Fp} creates open circuit voltage, $V_{oc} \approx \frac{E_{Fn}-E_{Fp}}{q}$[11]. The band-diagram shown in Figure 2.4 represents the separation in the quasi-Fermi level.

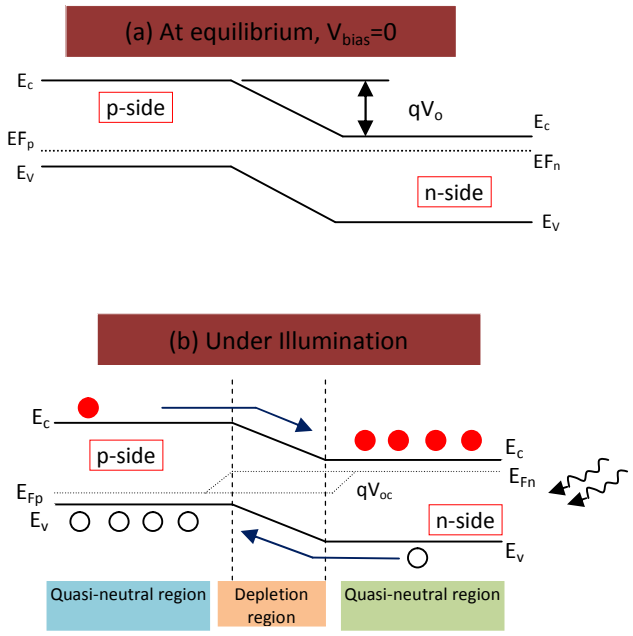

Figure 2.4 Band-diagram representing solar cell operation (a) at equilibrium, and (b) under illumination[11].

The generated electrons move towards the top cathode and the holes move towards the bottom anode as shown in Figure 2.4. Under illumination, the electron-hole pair generation increases the minority carrier concentration and the diffusion current dominates due to the concentration gradient developed in the quasi-neutral region. The direction of the photo generated current

density (J_{ph}) that flows from n-terminal to p-terminal is defined based on the flow of generated minority carriers. Collection of all the negative charges on the n-side and the positive charges on the p-side creates a light-induced forward bias to the solar cell[12]. In the existence of an external load, the diode current that is referred as the diode dark current, J_{dark} begins to flow in the opposite direction to the photo generated current[9]. The dark current reduces the photo generated current and it should be minimized. Diode current measurements provide information about the recombination mechanism in the solar cell that limits its performance.

Minority carrier diffusion length (L_n or L_p) is the most important solar cell material parameter. It depends on the minority carrier lifetime (τ_n or τ_p) and minority carrier diffusion coefficient (D_n or D_p) [8].Their relationship is given by:

$$L = \sqrt{D\tau} \qquad (2.2)$$

$$\frac{D}{\mu} = \frac{KT}{q} \qquad (2.3)$$

These parameters are important during the design of cell thicknesses and doping. Maximizing the diffusion length allows the minority carriers to reach their respective majority carrier side for collection to the external circuit. The cell thicknesses are designed in accordance with the minority carrier diffusion lengths[8]. These parameters are also dependent on the doping concentration.

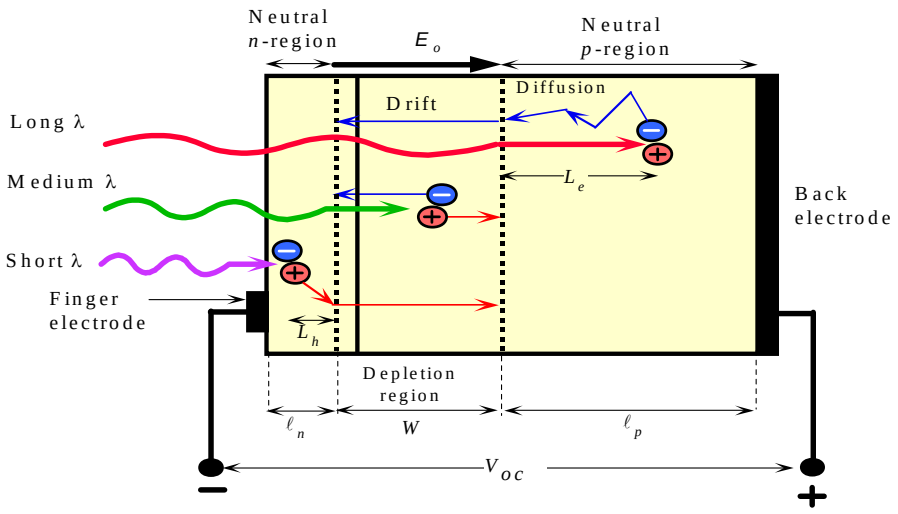

Figure 2.5 Photovoltaic Device Principle [8].

2.3 Characteristics of Solar Cells

The output current (J) of a solar cell under illumination is expressed as:

$$J = J_0 \left(e^{\frac{qV}{nKT}} - 1 \right) - J_{ph} \qquad (2.4)$$

where J is the current density, Vis the voltage, J_{ph} is the photo generated current density, J_o is the diode saturation current density, η is the diode ideality factor, *k* is the Boltzmann's constant and T is the temperature[9]. The first term of equation 2.4 represents the diode dark current (J_{dark}). The photo generated current density J_{ph} is nearly equal to the short-circuit density, J_{sc} of a solar cell.

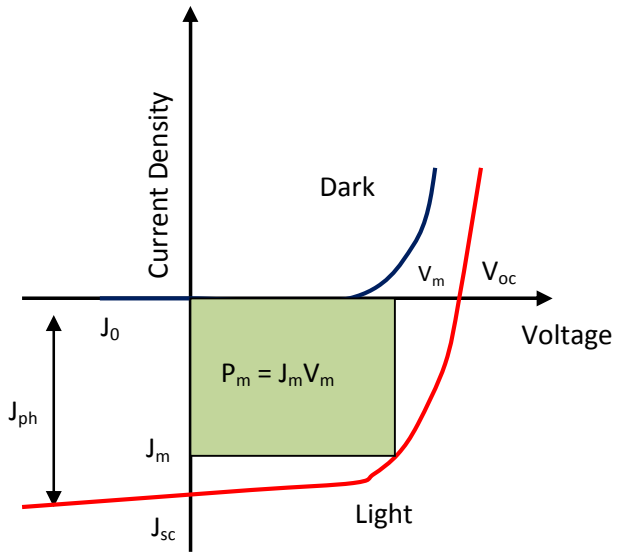

Figure 2.6 Current-Voltage (IV) characteristic of a solar under illumination and dark[12].

Figure 2.6 shows the current-voltage (IV) characteristic of a solar cell under illumination (red curve) and under no illumination (blue curve). In a good solar cell, the dark current is much lower than the photo generated current. The two mechanisms that contribute for dark current are n=1 and n=2 (n is the ideality factor)[12]. The recombination in the quasi-neutral region of the solar cell is represented by the ideal diode current (n=1), while the carrier recombination in the depletion region of the solar cell is represented by the depletion region dark current (n=2) accounts. Thus, the overall dark current is represented as follows:

$$J_{dark} = J_{01} e^{\frac{qV}{n_1 KT}} - 1 + J_{02} e^{\frac{qV}{n_2 KT}} - 1 \qquad (2.5)$$

where the first term represents the ideal diffusion dark current density and the second term represents the depletion region recombination current density.

The probability of an incident photon to generate an electron-hole pair that can be collected as external photocurrent is called the quantum efficiency (QE)of a solar cell. The internal quantum efficiency, IQE of the solar cell subtracts the reflectance component from the QE[9]. The quantum efficiency of a cell depends on absorption coefficient, material quality, and the cell capability to separate and collect the carriers. The short-circuit current density, J_{sc} of a solar cell is related to the quantum efficiency, QE as:

$$J_{sc} = q \quad b_s \; E \; . QE \; E \; . dE \tag{2.6}$$

where *q* is the elementary charge and b_s *(E)* is the incident photon flux density, i.e., the number of photons with energy in the range of *E* and *E+dE* incident on a unit area per unit time[9].

Under illumination, the minority carrier concentration significantly increases and causes quasi-Fermi levels split [11]. The open-circuit voltage, V_{oc} that is the maximum potential difference across the solar cell under open-circuit condition is created due to this split in the quasi-Fermi levels and expressed as:

$$V_{oc} = \frac{nKT}{q} ln \; \frac{J_{sc}}{J_0} + \; 1 \tag{2.7}$$

The resistance of the load that is chosen to maximize both the current and voltage ensure maximum power of the solar cell[2]. This point at which this output power is maximized is called the maximum power point, P_m and can be expressed as:

$$P_m = J_m V_m \tag{2.8}$$

where J_m and V_m are the current density and voltage at the maximum power point, respectively. The shaded region in Figure 2.6 represents the maximum power point. The fill-factor (*FF*) is major solar cell parameter that measures the quality or the “squareness” of the IV curve of a solar cell and expressed as [12]:

$$FF = \frac{P_m}{J_{sc}V_{oc}} = \frac{J_m V_m}{J_{sc}V_{oc}} \tag{2.9}$$

The ability of a solar cell to convert incident photons into output electrical power is defined as the efficiency of a solar cell (η)[4]. It can be represented as the amount of maximum power density delivered (P_m) as a fraction of the incident sunlight power density (P_{in}) and expressed as:

$$\eta = \frac{P_m}{P_{in}} = \frac{J_m V_m}{P_{in}} = \frac{FF J_{sc} V_{oc}}{P_{in}} \qquad (2.10)$$

The equivalent circuit model of a solar cell with the series resistance (R_s) and shunt resistance (R_{sh}) element is shown in the Figure 2.7[2] and the total current density in a solar cell taking into account the influence of R_s and R_{sh} is expressed as:

$$J = J_L - J_o \exp\left(\frac{V + JR_s}{nKT/q}\right) - \frac{V + JR_s}{R_{sh}} \qquad (2.11)$$

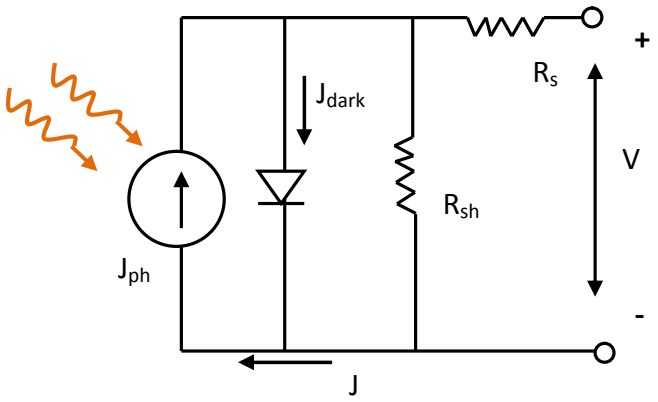

Figure 2.7 Equivalent circuit model of a solar cell under illumination[2].

2.4 Solar Cell Device Structure

Solar cells are formed by p-n junction semiconductors. A schematic of 1Junction n+/p solar cell is shown in figure 2.8[11]. The emitter layer, that is illuminated first, is heavily doped and thinner than the base layer. The light absorption in a solar cell mainly occurs in the base layer; which is thicker and lightly doped. Lower doping makes sure there is higher minority carrier lifetime, higher diffusion coefficients, and enhances the carrier diffusion length[13]. Moreover, lower doping in the base enlarges the depletion region in the base and assists carrier collection due to the electric field.

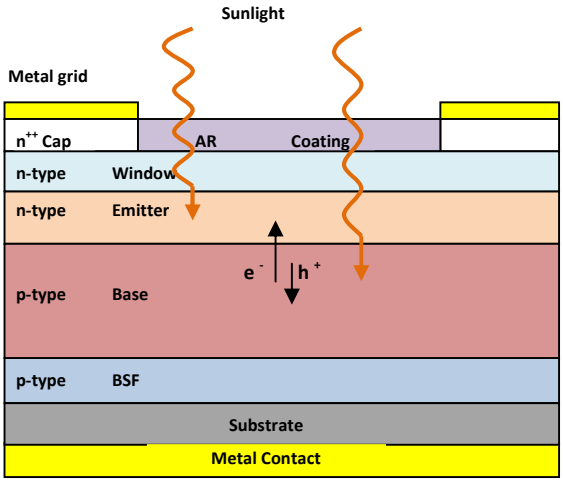

Figure 2.8 Cross-sectional schematic of 1Junction n+/p Solar cell [11].

The window and back surface field (BSF) are heterostructures, which are designed to reduce the recombination at the interfaces by passivation of the dangling bonds. Dangling bond occurs when an atom is missing a neighbor to which it would be able to bind. In addition, these heterostructures are chosen with appropriate band-offsets to reflect the minority carriers[11]. The window layer is intended to have a large valence band-offset to reflect the holes, whereas the BSF is intended to have a large conduction band-offset to reflect the electrons. These heterostructures are grown lattice matched to the cell and the semiconductor alloys used for them are selected to have higher band gap than the active junction material to lessen photon generation in these layers[12]. In addition, a solar cell consists back metal contact, front metal gridlines and an anti-reflective coating on the top surface.

A multijunction solar cell (2Junction, 3Junction...) comprise multiple individual sub cells stacked on top of each other to form a series connection. The individual sub cells are linked to each other through tunnel junctions[4]. The tunnel junctions are highly doped and designed to have very low series resistance. These junctions are very thin to allow the tunneling mechanism to rule the majority carrier transport. One of the most significant design criteria in optimizing the performance of a multijunction solar cell is attaining the current-matching condition between the sub cells. Current-matching allows to extract the best performance from a multijunction solar cell by enabling linear addition of the open-circuit voltages from the respective sub cells. By optimizing the doping and the thicknesses of various layers of each sub cell, current-matching

can be attained in multijunction solar cells[11]. The sub cell that generates least photocurrent restricts the overall cell performance due to the series connection.

CHAPTER 3

III-V SEMICONDUCTOR SOLAR CELLS

The III-V semiconductor solar cells are based on group III and group V elements as demonstrated in figure 3.1[14]. This common diagram shows the most interesting compounds for photovoltaic applications based on their band gaps and lattice constants.

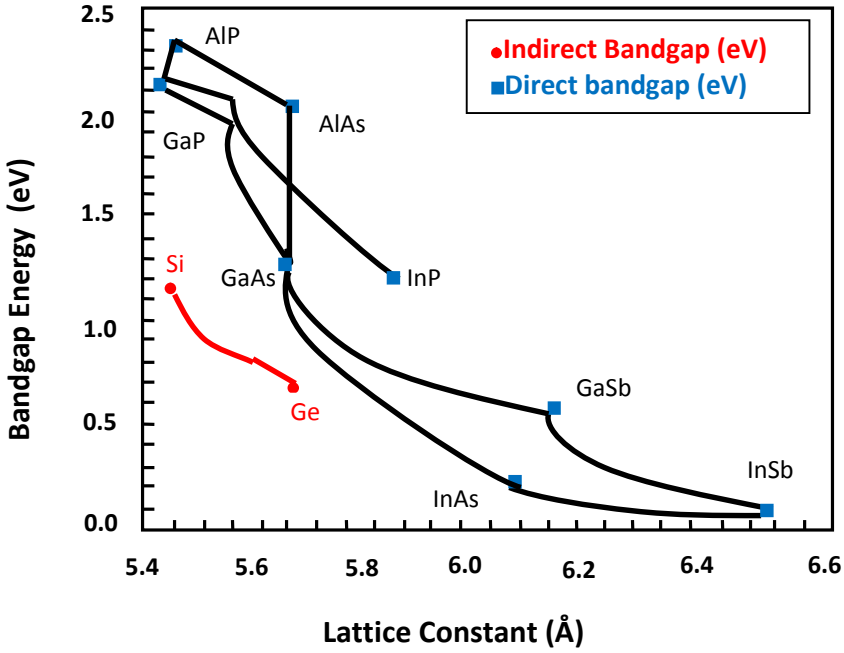

Figure 3.1 Semiconductor energy band gap versus crystal lattice constant[14].

The above figure shows the band-gap vs. lattice constant and gives an overview of different compound semiconductor alloys that can be made by carefully engineering the band-gaps and lattice constants in a device design[15]. The Bandgap energy in the electronic band structure is the energy difference between the top of valence band and the bottom of conduction band; the unit is electron volts (eV). Crystal lattice is the arrangement of atoms or group of atoms in a crystal. Crystals are composed of three-dimensional patterns; the patterns consist of atoms in ordered or symmetrical arrangements which are repeated at regular intervals keeping the same orientation to one another[14]. The simplest repeating unit in a crystal is called a unit cell. The lattice constant refers to the constant distance between the unit cells in a crystal lattice; the unit is Angstrom (Å)[13].

The concept of matching lattice parameters between the crystal film and the substrate is an important aspect of epitaxy. Epitaxy means the growth of a single crystal film on top of a crystalline substrate. If the film lattice parameter is the same as the substrate, they are called lattice matched. If there is a lattice parameter mismatch between the film and the substrate, the film material may strain to accommodate the lattice structure of the substrate. If strain accommodation is not possible then dislocation defects at the interface may form leading to relaxed epitaxy and the film returns to its original lattice structure above the interface[16]. The mismatched lattice parameter is called metamorphic.

Based on energy location in momentum space, there are two types of semiconductors; direct band gap and Indirect band gap semiconductor[13]. In the direct band gap semiconductors, minimum energy of the conduction band lies directly above the maximum energy of the valence band in momentum space. Electrons at the conduction-band minimum can combine directly with holes at the valence band maximum, while conserving momentum. In the indirect band gap semiconductors, the momentum of the conduction band minimum and valence band maximum are not the same, so a direct transition across the band gap does not conserve momentum and is forbidden. Recombination occurs with the mediation of a third body, such as a phonon or a crystallographic defect[8], which allows for conservation of momentum.

The gap between the photon energy and the bandgap energy Eg of the photovoltaic material is a main factor of energy loss[12]. If the photon energy is smaller than the bandgap energy, there will be no absorption. If the photon energy is much greater than the bandgap energy, the part that is equal to the bandgap energy will be absorbed and the other part will be wasted as heat. Multi-stacking of III-V group photovoltaic materials of different bandgap energies is used to minimize this energy loss and absorb the photon energy from the sunlight spectrum widely and efficiently.

The III-V compound semiconductor materials can be stacked on top of each other following the same crystal lattice. The flexibility in band-gap selection of III-V materials provides freedom during solar cell design through metamorphic or lattice-matched configurations[17]. Figure 3.2 shows that the multiple solar cells stacked on top of one another in III-V multi-junction solar cells allow a much broader absorption of the incident solar spectrum compared to the

conventional single-junction (1J) Si solar cells. When the multiple III-V solar cells with the same photo-currents are connected in series, the linear addition of the voltages from the individual sub cell gives higher conversion efficiencies.

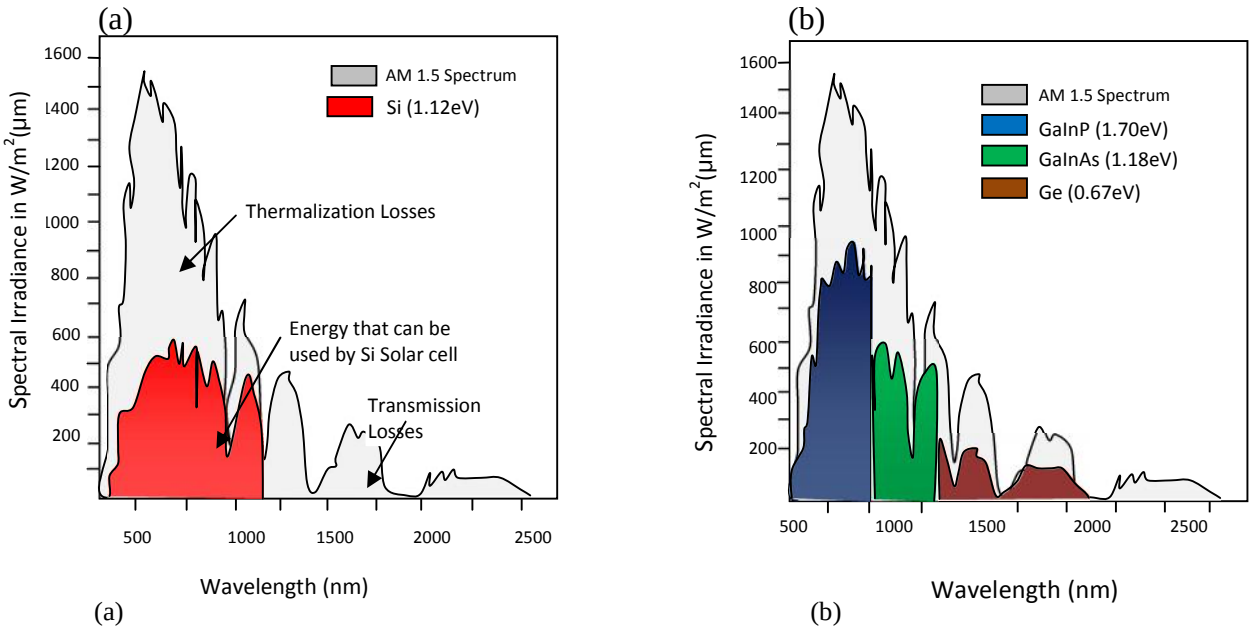

Figure 3.2 AM1.5 spectrum and the parts of the spectrum that can be used by (a) Si solar cells and (b) $Ga_{0.35}In_{0.65}P/Ga_{0.83}In_{0.17}As$/Ge solar cells[17].

III-V semiconductor solar cells have shown the leading energy conversion efficiencies, compared to the other materials[18]. Besides, the III-V semiconductor compound materials have advantages including the band gap tunability by elemental compositions, higher photon absorption by the direct band gap energies, higher resistivity against high-energy rays in space, and smaller efficiency degradation by heat[19]. III-V compound semiconductor solar cells have shown performance enhancement at approximately 1% (absolute) increase per year, with a recent record efficiency of 44.7%[5], while the performance of Si based solar cells have almost saturated at an efficiency (η) of 25% [6].

From binary material family, ternary and quaternary compounds can be achieved by substituting a range of fractions of different group III and group V atoms. Considering GaAs materials family, the ternary compound, $Al_xGa_{1-x}As$ is the first widely studied material[20-22]. It has a direct bandgap greater than GaAs in the compositional range; and it is nearly lattice matched to

GaAs across the entire range of Al fractions (Fig. 3.1). Residual strain can be avoided with the addition of a small amount of phosphorus during lattice matched $AlAs_{0.96}P_{0.04}$growth on GaAs. However, these compounds are unstable and highly reactive with increasing Al composition [21]. So, their use is limited to window layers, and tunnel junctions in photovoltaic cells[23]. There are other less reactive Al ternary and quaternary compounds like AlInP with gaps greater than GaAs. AlInP compound is lattice matched to GaAs and an important window layer preferred to AlGaAs due to its lower reactivity.

Considering phosphides, the ternary compound $Ga_{0.515}In_{0.485}P$ is lattice matched to GaAs[24]. The gap of this material varies as a function of sub lattice ordering: an ordered group III lattice yields a direct gap of 1.96eV, which is reduced, depending on the degree of disorder, by up to 0.5eV.

For bandgaps lower than GaAs, there is a shortage of interesting III-V compounds well-suited with GaAs. The quaternary solution $In_{1-x}Ga_xN_yAs_{1-y}$ has been proposed [25], as the addition of a few percent of nitrogen allows lattice matching and an ideal third junction bandgap. However, it brings crippling materials defects that lead to short minority carrier lifetimes [26]. Despite slow progress for some time, a breakthrough has been achieved by Sabnis *et al.* of Solar Junction, with the pentenary GaInNAsSb. [27]has reported an independently verified world record efficiency of 43.5% at 400 suns.

3.1 Substrates for III-V Solar Cells

The four most readily available semiconductor substrates are GaAs, Ge, InP and Si[12]. These substrates place restriction on the selection of band-gap and lattice-constant during optimal solar cell design.

Materials which are lattice matched with these substrates that can be grown without strain relaxation and associated defects are highly required to enhance device performance[28]. GaAs substrate is mainly used for single and dual Junction III-V solar cells with GaAs or lattice matched compound bottom active layer[29]. Ge is nearly lattice matched with GaAs and a small amount of In to GaAs allow exact lattice matching to Ge substrates[30]. Ge is usually used in triple designs as substrate and the lowest bandgap component[31].

Concerning substrates of InP, only the ternary $In_{0.53}Ga_{0.47}As$ of bandgap approximately 0.72eV is lattice matched to it. This is a non-ideal bandgap combination for multi-junction designs. This is due partly to inherent performance issues, and to the fact that InP is a relatively dense and rather brittle material [32,33] and therefore poses handling difficulties making industrial low cost development challenging.

The quaternary compound GaInAsP is lattice matched to all main substrates and it's the most attractive material family. It comprises as subsets the three important ternary phosphides which are GaAsP, GaInP, and InAsP, as well as all the important GaInAs materials family, essential in a wide range of applications[34]. This overview of materials leads to that compounds of the GaInAsP family on GaAs and Ge substrates are the most promising.

The Si substrate is used in order to reduce the cost of III-V solar cells. This substrate is used for Si and GaAs active layer. The feasibility of III-V solar cells on Si relies on the ability to grow high quality GaAs on Si with careful lattice engineering and substrate treatment. The lattice-mismatch makes the growth of GaAs on Si very challenging, rendering the metamorphic solar cell sensitive to defects including dislocation.

3.2 Design concepts of III-V Solar Cells

In solar cells under illumination, extrinsic losses such as reflection or external resistance, and intrinsic, such as optical and electrical transport losses are the main losses and recognizing these losses helps to improve the design [35].

The poor light-matter interaction and inefficient light absorption results in optical losses[35]. The transport losses can be expressed under the umbrella of finite carrier lifetimes and corresponding recombination loss via a range of channels[36].

3.2.1 Light and heat

The photon energy lower than the bandgap energy of the cell is transmitted without absorption. This is the first category of optical losses and it is shown in figure 3.3[37]. It indicates the part of the incident AM1.5G spectrum with energy below the bandgap that is transmitted through a cell. The resulting transparency loss as a function of bandgap is illustrated in Figure 3.4. This loss is small for low gap materials and rises with increasing bandgap.

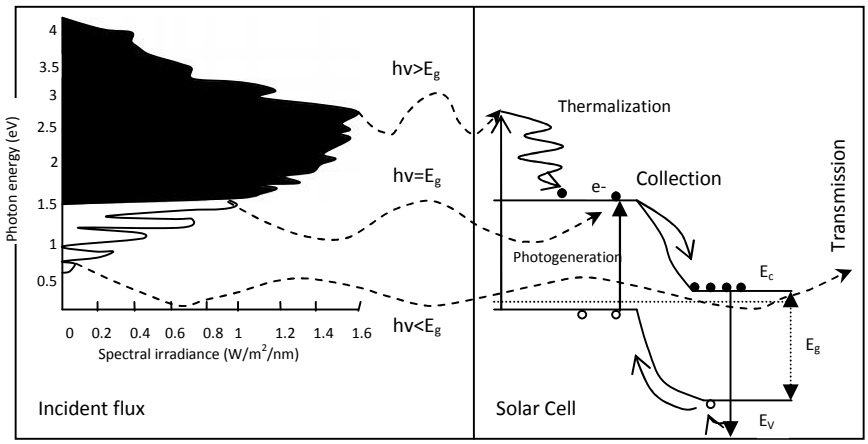

Figure 3.3 Illustration of losses with respect to the AM1.5G spectrum in a GaAs cell[37].

The next fundamental loss is thermalization (Figure 3.3) whereby carriers photo-excited with energies greater than the bandgap *Eg* rapidly thermalize, mainly via collisions with the lattice, establishing a steady state minority carrier population with a quasi-Fermi level (QFL) near the band-edge[37]. The photo-generated carriers are harvested with a fixed energy close to that of the lowest energy photons absorbed, wasting the remainder largely as heat. The resulting loss is shown in Figure 3.4.

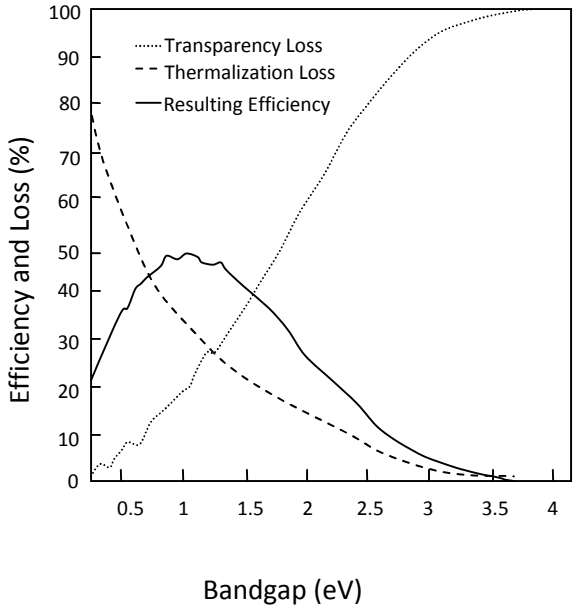

Figure 3.4 Effects of thermal and transmission losses on single junction solar cell efficiency[37].

3.2.2 Charge neutral layers

The first transport loss is the well-known Shockley injection current[10] in the dark, whereby majority carrier electrons and holes diffuse from an *n* or *p* region across the built in potential or junction bias under a concentration gradient and against the junction potential. They diffuse into a charge neutral region where they are minority carriers, and therefore recombine, giving rise to a net current. The diffusion or injection rate is a function of how long the diffusing carriers remain as minority carriers before recombining. The faster they recombine, the faster they are replaced, thereby increases the injection current[38]. This is characterized by hole minority carrier lifetimes τ_p in the *n* doped charge-neutral region and likewise τ_n for electrons in the *p* doped charge-neutral region. Via the Einstein relations $L_n = \tau_n D_n^{1/2}$ and $L_p = \tau_p D_p^{1/2}$ in terms of electron and hole diffusion constants D_n, D_p respectively, and diffusion lengths L_n, L_p across charge neutral widths x_p and x_n. The complete expression [39] for the dark current density at bias *V* can be expressed as

$$J_s\ V = q\ e^{\frac{qV}{K_B T}} - 1 \quad \frac{{n_{ip}}^2}{N_A}\frac{D_n}{L_n}\ \frac{\frac{S_n L_n}{D_n}\cosh\frac{X_p}{L_n}+\sinh\frac{X_p}{L_n}}{\frac{S_n L_n}{D_n}\sinh\frac{X_p}{L_n}+\cosh\frac{X_p}{L_n}} + \frac{{n_{in}}^2}{N_D}\frac{D_p}{L_p}\ \frac{\frac{S_p L_p}{D_p}\cosh\frac{X_n}{L_p}+\sinh\frac{X_n}{L_p}}{\frac{S_p L_p}{D_p}\sinh\frac{X_n}{L_p}+\cosh\frac{X_n}{L_p}} \qquad (3.1)$$

where $n_{ip}$is the intrinsic carrier concentration in the *p* layer doped at a level N_A, of surface recombination velocity S_n, and corresponding parameters n_{in} and N_D in the *n* doped later with its recombination velocity S_p.

3.2.3 Space charge region

The space charge region (SCR) or non-radiative recombination dark current can be expressed in terms of hole and electron diffusion profiles extending across it. This is the Shockley-Read-Hall (SRH) formalism[40] which may be expressed analytically in terms of carrier densities *n* and *p* as a function of depletion layer extending from $x_1$to $x_2$giving the following SRH recombination current density.

$$J_{SRH}\ V = q \int_{x_1}^{x_2} \frac{p\ x\ n\ x - {n_i}^2}{\tau_n(p\ x + p_t) + \tau_p(n\ x + n_t)}\ dx \qquad (3.2)$$

This current describes the non-radiative recombination considering only mid-gap trap levels (the most efficient for recombination) ,a space-charge layer with trapped electron and hole densities n_t and p_t, and electron and hole non radiative lifetimes τ_n and τ_p, respectively[38].

In the space charge region under illumination, the injected majority profiles are perturbed by a small population of free carriers collected at the depletion edges, and of free carriers photo generated in the SCR. The transport of these excess free carriers is dominated by drift, and lifetimes much greater than the short transit time across the depletion layer[10]. For this reason, the photocurrent contribution from the space charge region is assumed equal to the integral of the generation rate over that region. The sum of this SCR photocurrent and the charge-neutral contributions defines the total photocurrent J_{PH}.

3.2.4 Radiative losses

The last loss mechanism is the radiative loss[41], which applies in some measure to both charge neutral and SCR regions. This is the loss that is a direct consequence of absorption, and sets the fundamental limit on the efficiency of solar cells.

The generalized Planck equation expresses light emitted by a grey-body[42] as a function of absorption, geometry, and chemical potential or QFL separation of recombining species. It defines[43] the total current density J_{RAD} corresponding to the emitted luminescent flux at bias V from a radiative emitter as an integral over the photon energy E and surface S as

$$J_{RAD}\ V\ = q\ \int_0^{\infty} \frac{2n^2}{h^3c^2}\ \frac{E^2}{e^{\frac{E-q\Delta\emptyset}{KT}}-1}\ \int_s^{\infty} \alpha\ E,\theta,s\ dS\ \ dE \qquad (3.3)$$

where n is the refractive index of the grey-body, $\Delta\varphi$ is the quasi-Fermi level separation (the difference between hole and electron QFLs, and the other symbols have their usual meanings. The absorptivity $\alpha(E,\theta,s)$ is the line integral over position through the different layers of the cell along the optical path of radiation at angle θ with the normal exiting or entering surface S, the total emitting surface in three dimensions [42]. Therefore, J_{RAD} is minimized by reducing S, for example by coating the cell with reflective materials except on the absorbing fraction of the cell's surface facing the sun. This incidentally increases light trapping and is closely related to photon recycling concepts.

3.2.5 Resulting analytical model

The sum of contributions from charge neutral *p*, and *n* zones, and space charge regions gives the total photocurrent density J_{PH}[37][75]. This defines the external quantum efficiency including reflection loss (QE) as ratio of collected carriers to number of incident photons at a given wavelength, that is, the probability that a photon incident on the solar cell gives rise to a charge carrier collected at the cell terminal.

Finally, the light current density under applied bias, assuming superposition of light and dark currents is given by

$$J_L\ V\ = J_{PH} - J_S + J_{SRH} + J_{RAD} \qquad (3.4)$$

This light enables in the standard manner [11] to evaluate solar cell figures of merit such as the short circuit current $J_{SC} = J_L(0)$, the maximum power point V_{MP}, fill factor FF. Effects of parasitic resistance are included when modeling real data in the usual manner, that is, a series resistance defining a junction bias, and a parallel resistance and associated shunt current reducing the photocurrent.

CHAPTER 4

COMPARISON OF III-V SOLAR CELLS ON GaAs, Ge, Si SUBSTRATE

4.1 III-V Solar Cells on GaAs Substrate

4.1. 1 Single Junction III-V Solar Cells on GaAs Substrate

The single junction solar cell described below illustrates the concepts developed in chapter 3.

Figure 4.1 shows the spectral response for 25% efficient GaAs *solar* cell on GaAs substrate[44].

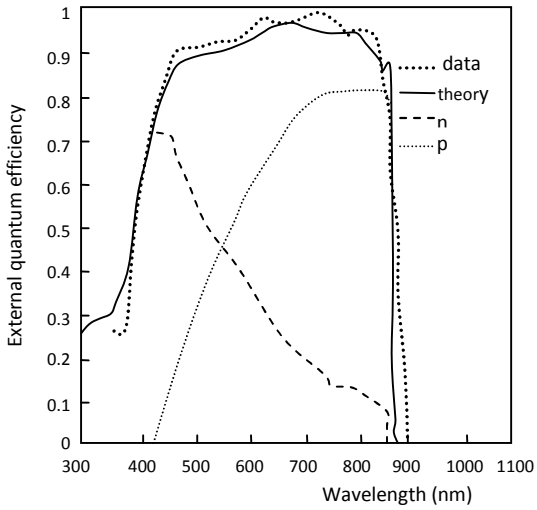

Figure 4.1 Spectral response of GaAs cells[44].

The 25% *np* cell shows considerably higher short wavelength response; however the short wavelength QE is dominated by less efficient hole minority carrier collection in the n-type emitter layer. This is due to the main novelty of this cell, which is the use of a 30nm GaInP window on a thin 0.1µm n-type emitter. Because of the novel window, there is very low emitter-window recombination velocity allowing a thin emitter without excessive spreading resistance and high collection efficiency in this thin n-type layer[44].

Figure 4.2 shows the complementary modeling in the dark, using the transport parameters consistent with the QE modeling. The left and right axes show respectively the dark current contributions and the resulting radiative efficiency.

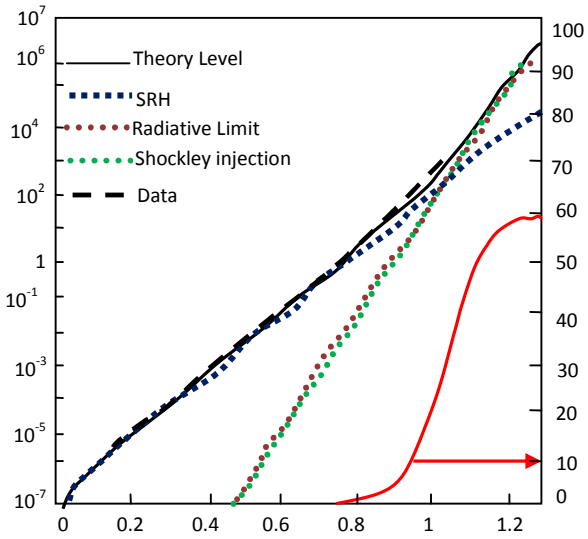

Figure 4.2 Dark current of a 25% efficient pn GaAs cell[44].

Table 4.1 Record GaAs cell parameters published by Kurtz [44] for AM1.5G compared with analytical model.

	J_{sc} (A/m^2)	V_{mp} (V)	V_{oc}(V)	FF(%)	Efficiency (%)
Kurtz	285	NA	1.05	85.6	25.0+0.8
Model	278	0.91	1.05	82.7	24

The modeling is consistent with available light and dark data and shows that the 25% record cell is radiatively dominated only at high bias. The radiative recombination from the SCR and charge neutral layers is 58% of the total as the cell approaches flat band. Besides, series resistance is negligible in this case, reflecting the high quality GaInP of window layer design and high conductivity of the solar cell surface layers with little loss of photogeneration.

There appears to be a consistent picture of the physical phenomena developed in describing these high purity crystalline solar cells. The dark current and light current modeling consistency leads to controlled modeling which gives detailed information concerning the operational regime of solar cells.

The highest efficiency achieved from lattice-matched thin film 1J GaAs under the global AM1.5 spectrum ($1000W/m^2$) is 28.8%[5].

Table 4.2 Record GaAs cell parameters published by A.Green et al [5] for AM1.5G

	J_{sc} (mA/cm^2)	V_{oc} (V)	FF (%)	Effic. (%)
A.Green	29.68	1.122	86.5	28.8±0.9

4.1.2 Dual Junction III-V Solar Cells on GaAs Substrate

The efficiency contour (Figure 4.3) shows that dual junctions may reach 42.2% without concentration[45] in terms of upper and lower gaps, assuming only radiative losses and a perfect, lossless tunnel junction. Non-ideal bandgap combinations may reach close to this efficiency. The contour shows that a tandem efficiency is insensitive to change in bandgap provided that both gaps are varied simultaneously. For example, a tandem with gaps (0.8, 1.6)eV will perform almost as the same as the one with gaps (1.19, 1.78)eV, with an efficiency of about 42%, both only slightly lower than the absolute maximum.

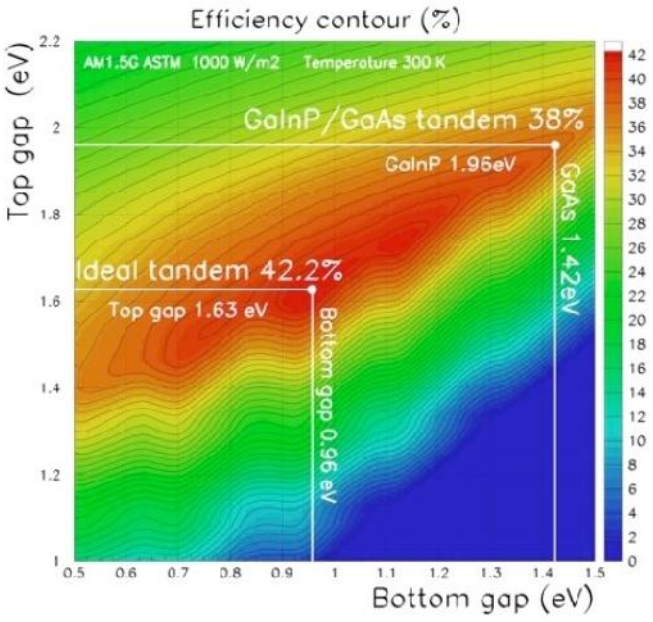

Figure 4.3 Ideal dual junction solar cell maximum conversion [45].

Considering the ideal limit, the upper and lower bandgaps for the maximum tandem efficiency of 42.2% are 1.63eV and 0.957eV, as shown on the Figure 4.3. For GaAs substrate, there are two materials with the higher gap (1.63eV) that are lattice matched to GaAs.

The first, $Al_xGa_{1-x}As$, from x=0 up to $Al_{0.49}Ga_{0.51}As$, a bandgap ranging from 1.424 to 2eV includes 1.63eV cell for a composition of approximately x=0.17.

The second material is in the $Ga_xIn_{1-x}As_yP_{1-y}$ family which ranges from 1.424eV (GaAs) to 1.9eV (that is, x=0.51, y=0.49) with a continuous range of group III and group V compositions lattice matched to GaAs. The flexibility of this quaternary has an advantage with the possibility to lattice match with Ge[37]. This phosphide material mainly studied on InP substrates for telecommunications applications[14], and received little attention on GaAs substrates due to the availability of AlGaAs which is historically well established, and easier to grow[46]. As the result, materials knowledge is largely restricted to the lattice matched ternary endpoint $Ga_{0.51}In_{0.49}P$, and that lattice matched quaternary materials are simply expressed by a linear interpolation as $(GaAs)_{1-z}(Ga_{0.51}In_{0.49}P)_z$. These considerations suggest that this quaternary materials family is worthy of greater attention. However, in the current state of knowledge, the quaternary composition $(GaAs)_{0.8}(Ga_{0.51}In_{0.49}P)_{0.2}$ has the correct direct gap of 1.63eV for ideal tandem structure, for which a lower gap 0.957eV material needed to be identified.

For this lower gap however there is no lattice matched candidate. Using GaAs, the lowest available gap, as the lower gap sub-cell of a tandem yields an ideal efficiency limit of 38%. This dictates an ideal upper sub-cell bandgap of 1.95eV, obtainable with AlGaAs but is generally not considered as a candidate for tandem cells[47]. The GaAs based tandem, however, remains a feasible design with a phosphide material which is nearly ideally matched by GaInP, and has the potential to reach 38% efficiency.

Returning back to the ideal tandem efficiency limit of 42%, the closest material with the correct lower sub-cell bandgap of 0.957eV is $In_{0.43}Ga_{0.57}As$. This compound is lattice mismatched to GaAs substrates, with a critical thickness of just 8nm after which misfit dislocations result in a serious penalty in cell efficiency[37].

Among the different works on multijunction cells, an analysis of a dual junction with GaAs/GaInP combination mentioned earlier with a theoretical maximum efficiency of 38% is presented here under. This dual junction solar cell has been tried by a number of groups and one of the first achieved over 30% under concentration of 100 to 200 suns in 1994[48]. The Takamoto paper reports over 30% efficiency under a global un concentrated spectrum[49].

The device structure of Takamoto's paper is *n* on *p* with an AlInP window layer. Like the Kurtz single junction cell, the n-type emitter is heavily doped and only 50nm thick, while the lightly doped base (hence with good minority carrier transport) is 0.55μm thick. The tunnel diode consists of nand *p* doped InGaP layers of 30nm each doped $10^{25}m^{-3}$ (Zn) and $0.8x10^{25}m^{-3}$ (Si) respectively, and sandwiched between higher gap AlInP cladding layers. These are intended, to minimize the common problem of dopant diffusion from the highly doped tunnel junction. The device is completed by a GaAs bottom junction with InGaP back surface minority carrier reflector[37].

Figure 4.4a shows the modeled QE assuming a double layer MgF_2/ZnS antireflection (AR) coat and showing a good fit overall. The breakdown of different regions clearly shows the dominance of photocurrent produced by p-type layers which gets advantage from better electron minority carrier transport than the n-type layers. In this *n* on *p* geometry, the more efficient *p* layer dominance is attained by using a thin *n* layer combining with good interfaces between the GaAs *n* layer and the tunnel junction cladding, and the topmost n-type GaInP layer and the AlInP window.

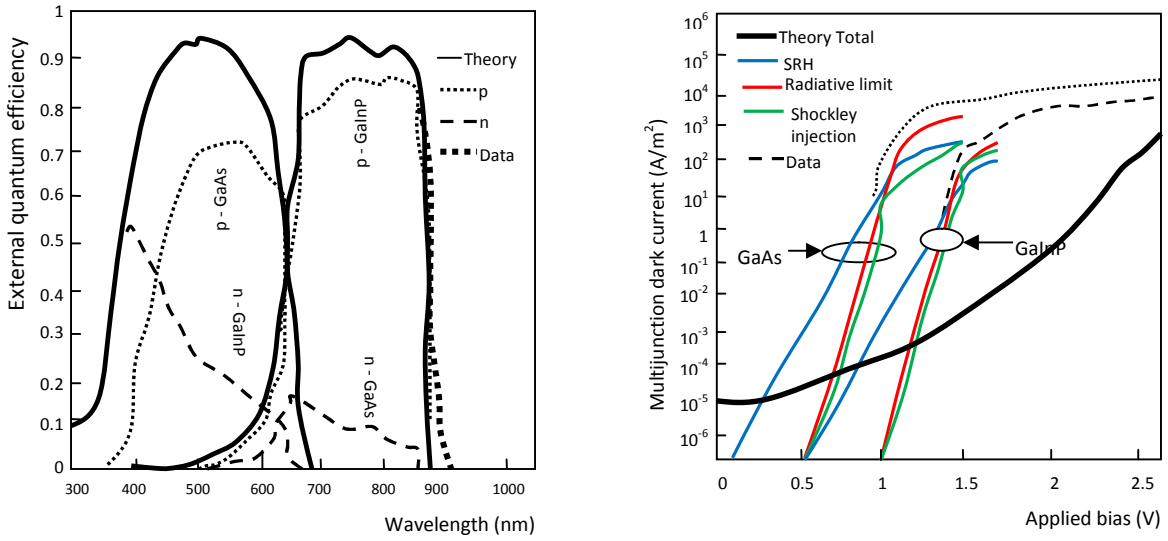

Figure 4.4(a)QE data and modeling showing the detail of layer contributions and (b) Dark current data and modeling for high efficiency GaInP/GaAs tandem[50].

The other main point to note is that the significant QE of the bottom GaAs cell above the GaInP bandgap: which implies that the top cell is somehow opaque near its bandgap. This is another design feature of this cell: In order to ensure current continuity in the light of the imperfect band-

gap combination imposed by the GaAs, the top cell is made thinner in order to ensure current continuity at the expense of a slightly greater thermalization loss in the GaAs cell.

Figure 4.4b shows the corresponding dark current fit together with individual subcell and overall tandem dark currents. The tandem current is determined by the sub-cell current-voltage characteristics by adding sub-cell biases at constant current assuming an ohmic tunnel junction. As mentioned earlier, this estimates the Shockley injection from the transport parameters, and calculates the radiative current from the cell geometry and absorption coefficient, both validated by the QE fit. In the case of the dark current there is, in this case, an imperfect fit and signs of systematic error at low bias, which cannot be elucidated further without separate dark IV curves for both subcells. At higher bias however, agreement is sufficient to indicate that the higher gap GaInP sub-cell is approximately 40% radiative, and the bottom GaAs sub-cell is approximately 65% radiative, comparable if slightly better than the Kurtz single junction cell reviewed previously.

The model results are compared with the published data in table 4.3. In this case, the model slightly under-estimates experiment, due to under-estimating the short circuit current density by about 2%, but more importantly because of over-estimating the dark current at high bias by a factor of up to 2 in the region of the V_{OC} at 2.5V. This can be seen in the under-estimated V_{OC} in particular.

Table 4.3 Tandem cell published parameters for AM1.5G compared with analytical model results [49].

	J_{sc} (A/m^2)	V_{oc}(V)	FF(%)	Efficiency (%)
JEC	142.5	2.49	85.6	30.3
Model	139.5	2.32	87.0	29.4

A record efficiency of 32.6% at 1000 suns has been demonstrated for the 2J InGaP/GaAs cell on GaAs substrate[51].

4.2 Triple Junction III-V Solar Cells on Ge Substrate

Figure 4.5 shows the schematic of triple junction solar cell[19] and Figure 4.6 shows the result of a numerical optimization of the three gap system efficiency in the radiative limit[45]. The efficiency contour is much sharper than the dual junction. Any variation from the ideal decreases the efficiency that cannot be corrected to the same degree by altering the other two bandgaps.

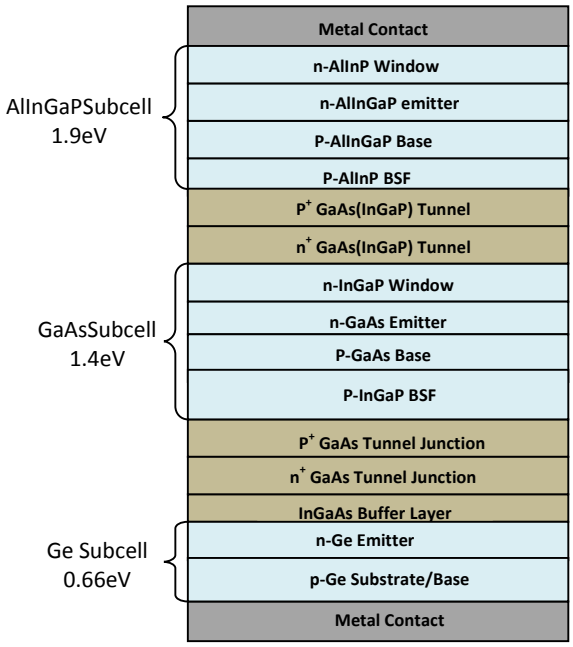

Figure 4.5 Cross-sectional schematic of 3-Junction Solar cell[19].

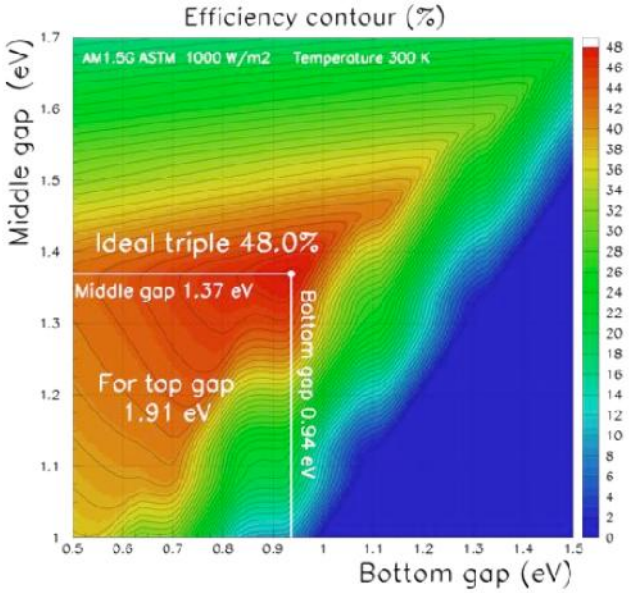

Figure 4.6 Ideal triple junction solar cell maximum conversion efficiency[45].

The ideal sub-cell bandgaps found for the triple multijunction cell are 1.91eV, 1.37eV and 0.94eV, which together give an efficiency of 48% [45]. Referring to Figure 4.6, the upper gap is well approximated by $Ga_{0.515}In_{0.485}P$ of gap 1.9eV which is lattice matched to GaAs, the middle gap cell at 1.37eV corresponds to $In_{0.05}Ga_{0.95}As$ which has a critical thickness of 70nm on a GaAs substrate, but there is a lack of lattice matched lower gap materials[45].

The survey of materials available in III-V semiconductors for ideal dual and triple junction cells shows that the wide range of materials require some additional tricks to circumvent materials issues resulting from mismatched materials. The brief study of available materials leads to that the most promising materials for both dual and triple junction designs are GaAs and GaInP, and lower gap material for the triple is not yet determined.

Table 4.4 gives a summary of ideal triple junction characteristics calculated in the radiative limit for AM1.5G global spectrum without concentration.

Table 4.4 Ideal triple cells gaps and efficiencies for standard global spectra[45].

Spectrum	Top gap	Mid gap	Low gap	J_{sc} (A/m2)	V_{oc} (V)	Eff. (%)
AM1.5G (1000W/m^2)	1.91eV	1.37eV	0.94eV	167.0	3.20	47.9

The materials limitations are stricter than the dual junction case. This is because triple junction efficiency is more sensitive to variations in bandgap, and the ideal bandgaps are far from available lattice matched materials.

In this context, these designs and their higher efficiencies have led to the development of lattice matched and heterogeneous growth III-V cells on Ge substrates. An example consisting of GaInP, GaInAs and Ge substrate subcells is provided by King *et al.*[52] where the reference includes the detailed cell structure together with lattice matched and mismatched cells.

The lattice matched material looks at the optimum material quality option, while the lattice mismatched, metamorphic option is intended to approach the ideal subcell bandgaps more closely. Besides, there is interesting degree of freedom, which is the use of group III sublattice disorder to control the bandgap, and thereby the current matching in the triple junction. The band

structure is not explicitly stated by King *et al.*[52]but is approximately (1.87, 1.40, 0.67) eV for lattice matched GaInP, $Ga_{0.99}In_{0.01}As$, and Ge subcells.

The optimal bandgaps in the ideal limit for a Ge substrate subcell are 1.88eV for the top GaInP subcell, and 1.33eV GaInAs middle gap sub-cell for a 0.67eV Ge subcell and substrate. The ideal one sun AM1.5G efficiency for this structure is 45.5%[45].

The GaInP may be engineered to match this with careful use of composition and order mentioned above. The ideal $Ga_{0.955}In_{0.055}As$ however cannot, but the tolerable critical thickness of nearly 3μmfor this layer[52] is the reason the metamorphic route is investigated in the King reference.

The net difference between the two cases is relatively minor, however, there is similar performance within margin of error. Therefore, the analysis is limited to the lattice matched case as a direct progression from the previous single junction and dual cases is examined.

The main interest is the study of ideality 1 and 2 mechanisms reported in the paper for both lattice matched and mismatched triple structures. The method used by King *et al.* is the probing of J_{sc} and V_{oc} as a function of cell illumination intensity. Subject to the assumption of the superposition principle, this yields the dark current for the upper GaInP and middle GaInAs subcells but not the low gap Ge subcell.

In relation to earlier discussion of the meaning of ideality 1 regimes, ideality n=1 regime is explicitly defined as the regime where the dark current is dominated by the Shockley injection current and concludes that the sub-cells increasingly approach the ideality 1 regime at high bias consistent with the modeling reported here.

Figure 4.7 shows the modeled QE for each subcell assuming a calculated reflectivity consistent with the published data. The modeling uses transport data from the literature,[14] validated by the good QE fit. The model shows that the Ge substrate bandgap is significantly below the optimum and this sub-cell over-produces current[52]. As a consequence, it is forced into forward bias in order to decrease its net current and achieve current parity and continuity with the other subcells. Therefore, it operates at lower efficiency at a bias beyond its maximum power point.

The other consequence of a non-ideal lower bandgap is excessive thermalization in this Ge sub-cell and consequent efficiency loss.

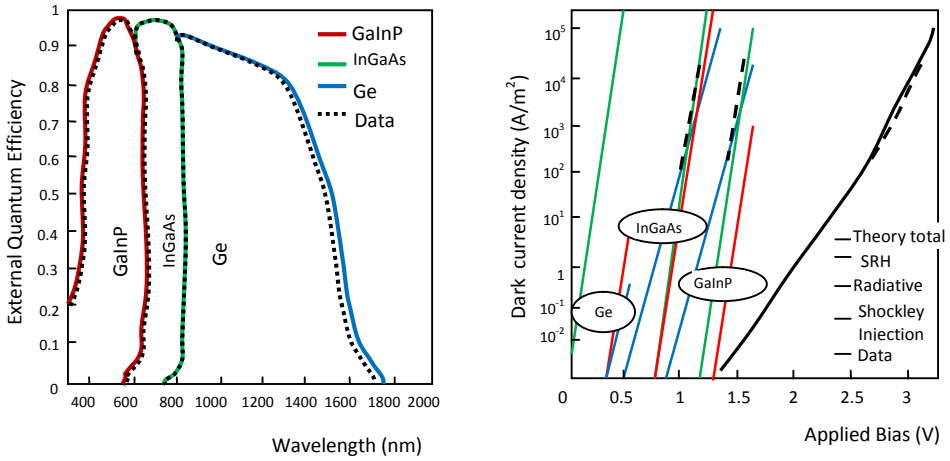

Figure 4.7(a) QE data and modeling for the three subcells of triple junction cell [52] and (b) dark current data and modeling for the subcells and the combined triple junction.

The dark current is shown on the right hand of Figure 4.7 for available sub-cell data and the overall experimental tandem response. The lack of Ge data leads to the use of transport data from the literature for this material that is validated by the good QE fit. The relatively short range of available dark current data for the GaInAs junction, GaInP junction, and overall triple junction device nevertheless covers the transition between the n≈2 and n≈1 idealities, together with the experimental maximum power point V_{mp} and V_{oc} reported[52]. For these three sets of data, the model provides a good fit subject to the proviso of short datasets.

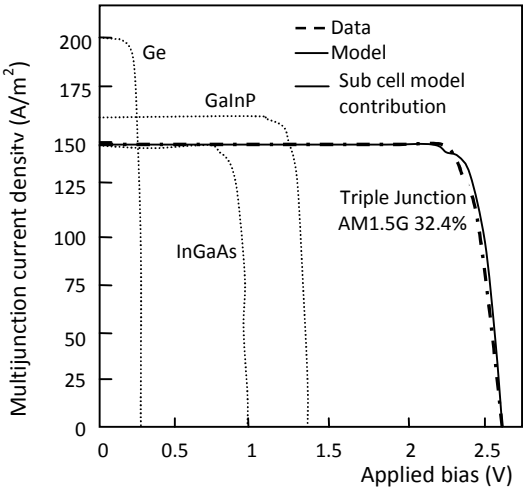

Figure 4.8 Multijunction current density[52].

Table 4.5 shows that the range of dark current data and modeling covers the illuminated maximum power point bias V_{mp}. It also covers the transition from non-radiative dominated ideality at low bias to the n=1 ideality marking the Shockley injection regime which may be radiatively dominated.

Table 4.5 Comparison of modeling and published parameters for the triple junction [52] lattice matched GaInP/GaInAs/Ge design under the AM1.5G spectrum compared with modeling.

	J_{sc} (A/m^2)	V_{mp} (V)	V_{oc}(V)	FF(%)	Efficiency (%)
King	143.7	2.30	2.62	85.0	32.0
Model	143.2	2.31	2.62	86.0	32.4

Following that, King *et al.* had grown and fabricated Metamorphic three-junction $Ga_{0.44}In_{0.56}P/Ga_{0.92}In_{0.08}As/Ge$ terrestrial concentrator solar cells with a graded buffer structure and low threading dislocation density under a wide range of experimental conditions[53]. Figure 4.9 plots the measured illuminated I-V curve for a record efficiency 40.7% metamorphic GaInP/GaInAs/Ge three-junction cell at 240 suns, under the standard spectrum for terrestrial concentrator solar cells(AM1.5D, 24.0 W/cm2, 25 °C).

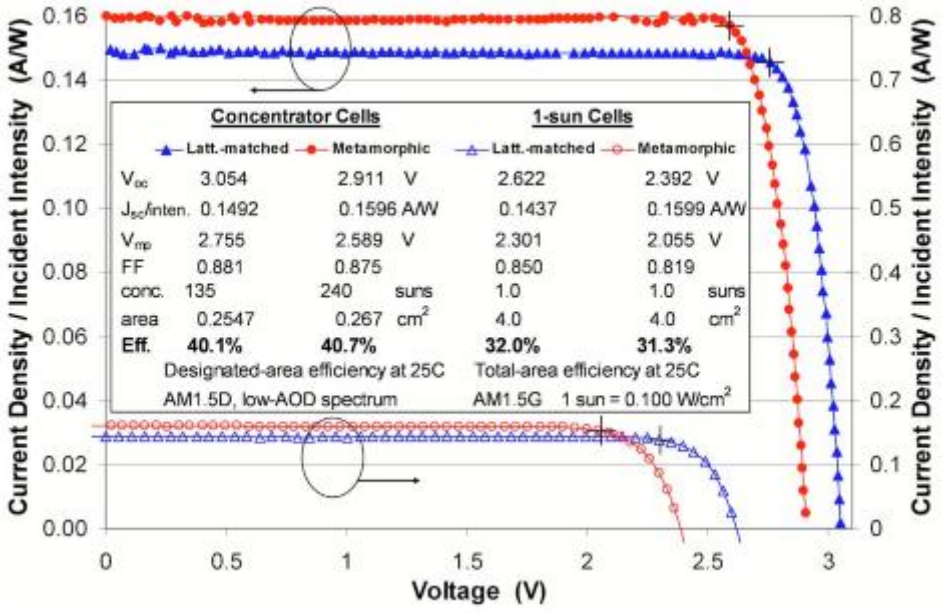

Figure 4.9. I-V characteristics of 3-junction solar cells under the concentrated terrestrial solar spectrum, and 1 sun cells[53].

The solar efficiency table (version 42) has released 44.4% conversion efficiency[5] with inverted metamorphic InGaP/GaAs/InGaAs structure in 302 sun.

4.3 III-V Solar Cells on Si Substrate

The feasibility of III-V solar cells on Si relies on the ability to grow high quality GaAs on Si with careful lattice engineering and substrate treatment. The lattice-mismatch makes the growth of GaAs on Si very challenging, rendering the metamorphic solar cell sensitive to defects including dislocation[12]. These dislocations generated due to mismatch between GaAs and Si can propagate into the photoactive cell region and significantly impede the minority carrier lifetime and hence the overall cell performance.

4.3.1 Single-Junction GaAs Solar Cell on Si Substrate

The schematic of 1J n+/p GaAs solar cell on Si substrate is indicated in Figure 4.10. In the analysis, the p-GaAs base thickness was 2.5μm at the beginning [30] and the TDD in this GaAs cell was varying from 10^4 cm^{-2} to 10^8 cm^2.

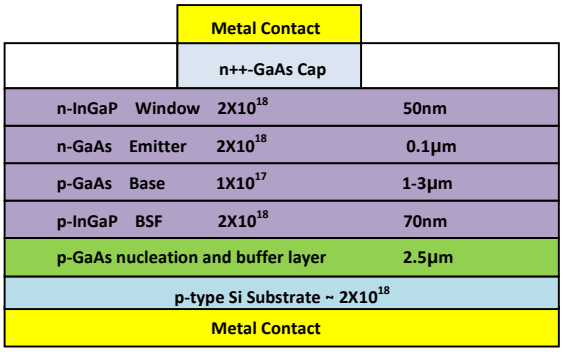

Figure 4.10 Schematic depiction of 1J GaAs Solar Cell on Si substrate [30].

As indicated in Figure 4.11, the calculated minority electron lifetime in p-GaAs at a TDD of 10^6 cm^{-2} was 1.49 ns[30], it's similar with the experimental result of minority electron lifetime; which is 1.5 ns in p-GaAs[54]. The 1J GaAs solar cell band-diagram under equilibrium is shown in Figure 4.12 and under illumination is shown in Figure 4.13[12]. Under illumination, there is split of Fermi level into the two quasi-Fermi levels on the n-side and the p-side.

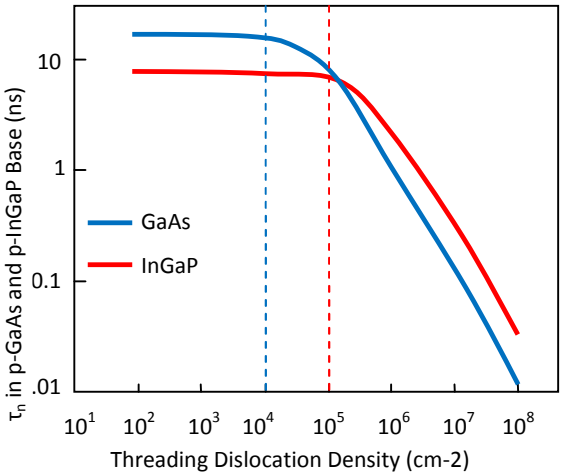

Figure 4.11 Correlation of TDD on the minority electron lifetime in p-GaAs and p-InGaP base[30].

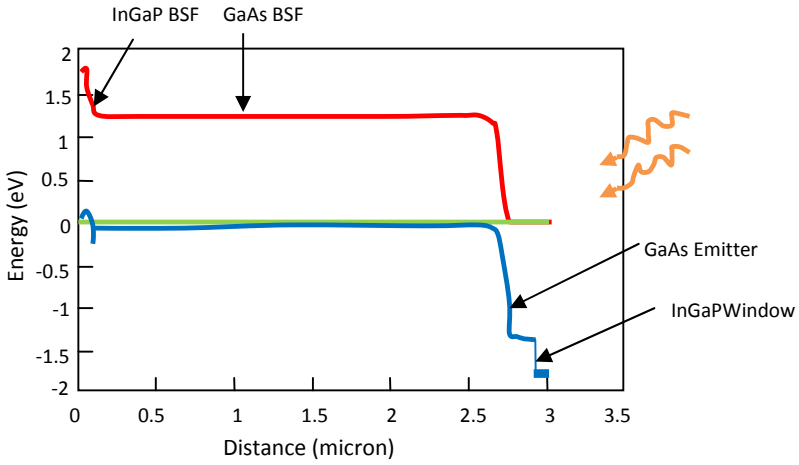

Figure 4.12 Band gap of 1J n+/p GaAs solar cell at equilibrium[12].

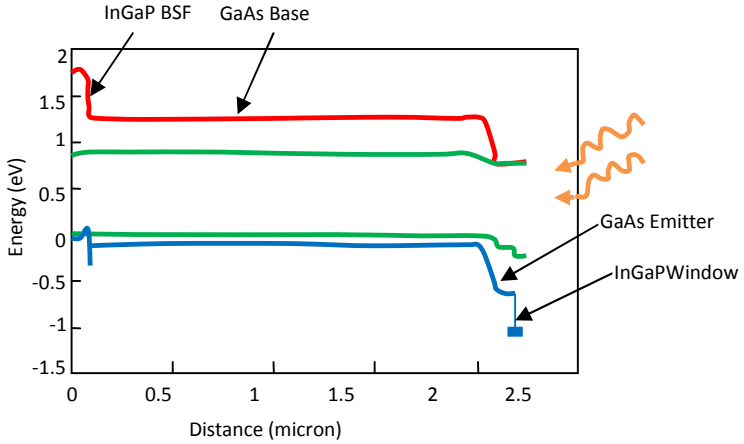

Figure 4.13 Band gap of 1J n+/p GaAs solar cell under illumination[12].

Figure 4.14 (a) shows Voltage at maximum power point, V_m and V_{oc} against the increment of TDD in the 1J GaAs cell on Si. V_{oc} and V_m have higher values at lower TDD due to the higher minority electron lifetime at lower TDD in the p-GaAs base[54]. The Epitaxial growth with TDD less than 10^4 cm^{-2} is considered as lattice-matched and a TDD below 10^5 cm^{-2} had insignificant impact on the V_{oc}. However, beyond this TDD, V_{oc} started to degrade significantly[55].V_{oc} has a logarithmic dependence on reverse saturation current density, J_0 which is inversely proportional to the minority carrier lifetime. Therefore, the lower values of V_{oc} and V_m at higher TDD was due to the higher reverse saturation current density relating to the reduced minority electron lifetime.

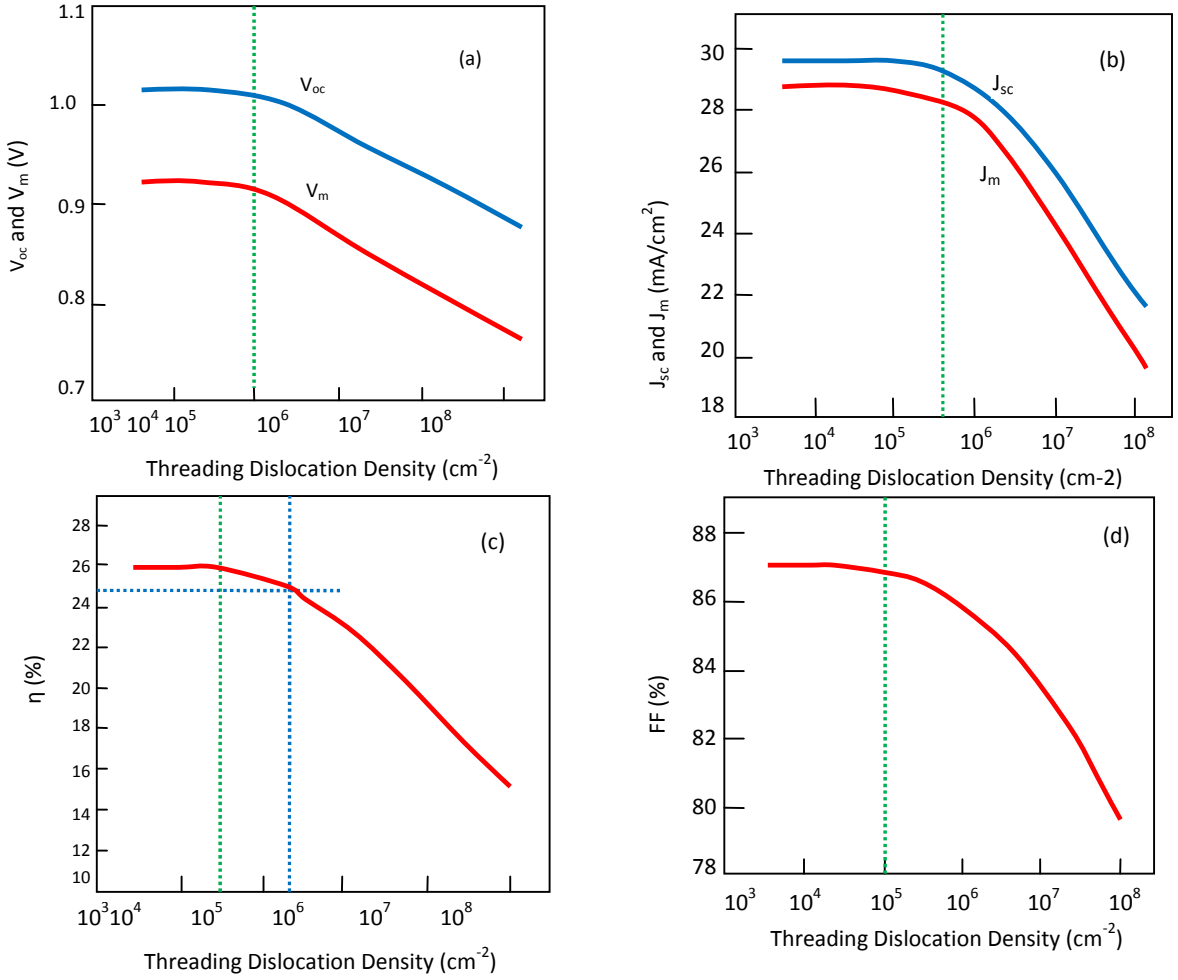

Figure 4.14 Impact of TDD variation on the performance of 1J GaAs solar cell on Si: (a) V_{oc} and V_m, (b) J_{sc} and J_m, (c) η and (d) FF under AM1.5G spectrum[55].

Figure 4.14 (b) shows current density at maximum power point, J_m and J_{sc} against the increment of TDD in the 1J GaAs cell on Si. The minority electrons had sufficient lifetime to reach the junction before being recombined at TDD below $4x10^5$ $cm^{-2}$and had insignificant impact on the J_{sc}[54].A minimum of 0.78ns minority electron lifetime (at a TDD of $2x10^6$ cm^{-2}) was required for 1J GaAs cell to function as a short diode and beyond a TDD of $2x10^6$ cm^{-2}, the cell acts like a long diode with the electron diffusion length becoming shorter than the GaAs base thickness[30]. Thus, J_{sc} and J_m have lower values beyond a TDD of $2x10^6$ cm^{-2} due to the reduction in minority electron lifetime. As shown in figure 4.14 (a) and (b), J_{sc} starts to decrease at a higher TDD than V_{oc}, indicating J_{sc} was more tolerant to TDD in the 1J GaAs solar cell on Si.

Figure 4.14 (d) shows the fill factor against the increment of TDD. There was negligible drop in fill factor for TDD lower than 10^5 cm^{-2}. The percentage drop in both J_m and V_m from a TDD of 10^4 cm^{-2} to 10^8 cm^{-2} was greater than the percentage drop in J_{sc} and V_{oc}, respectively, as indicated Figure 4.14 (a) and (b). Thus, at higher TDD, a greater percentage drop in the J_m*V_m product compared to $J_{sc}*V_{oc}$, led to the degradation in FF. This degradation in FF in turn restricted the performance of the 1J GaAs solar cell on Si at higher TDD.

Figure 4.14 (c) shows the degradation in efficiency of the 1J GaAs solar cell on Si as a function of increasing TDD. The cell efficiency greater than 25% was attained for TDD below $2x10^5$ cm^{-2} (or τ_n greater than 5 ns)[12]. The highest efficiency for this 1J GaAs cell was ~26%.Beyond a TDD of ~10^5 cm^{-2}, the cell efficiency lowered due to the reduction in both J_m and V_m. At an experimentally realistic TDD of 10^6 cm^{-2}, the corresponding cell efficiency was found to be 23.54%[55], about an absolute 3% lower efficiency when the cell had minimal dislocations. At a higher TDD of 10^7 cm^{-2}, the corresponding cell efficiency degraded to 19.61% due to the radical reduction in the minority electron lifetime[30]. This efficiency was about an absolute 6% lower than the performance of the lattice-matched GaAs solar cell, thus, suggesting that 1J GaAs solar cell are extremely sensitive to threading dislocations.

4.3.2 Dual-Junction InGaP/GaAs Solar Cells on Si Substrate

The base thicknesses in the GaAs and InGaP subcells were set to 2.5µm and 0.9µm, respectively to analyze metamorphic 2J n+/p InGaP/GaAs solar cell on Si[30]. Figure 4.15 shows the schematic of the 2J InGaP/GaAs solar cell structure on Si and Figure 4.16 (a) and (b) show the corresponding band-diagrams at equilibrium and under illumination respectively. It was assumed that all the threading dislocations in GaAs bottom sub cell transmitted to the top InGaP subcell even if the top InGaP sub cell grown lattice-matched to the bottom GaAs sub cell[30]; the TDD was varied from 10^5 to 10^8 cm^{-2}.

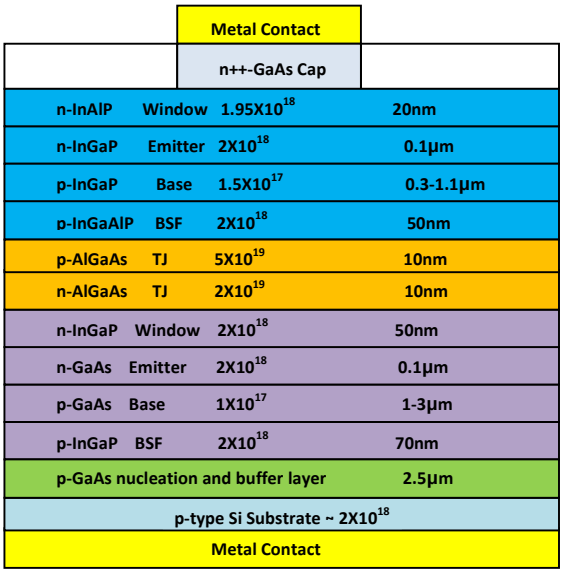

Figure 4.15 Schematic depiction of 2J InGaP/GaAs Solar Cell on Si substrate[30].

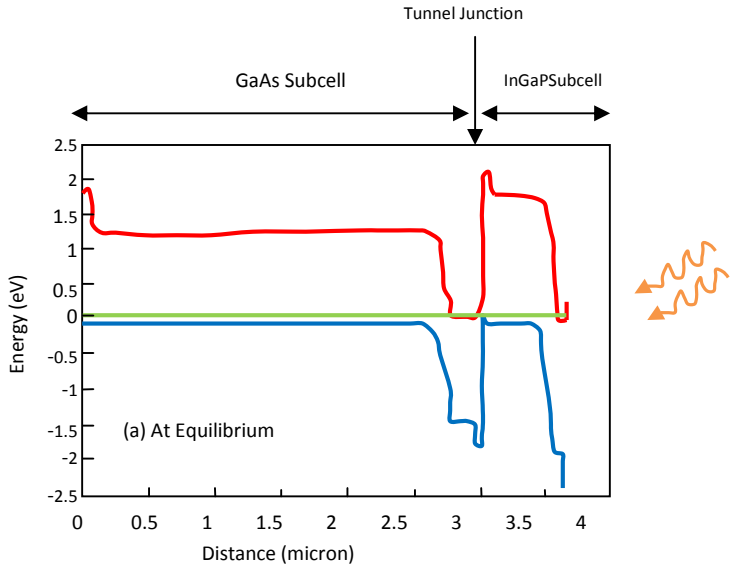

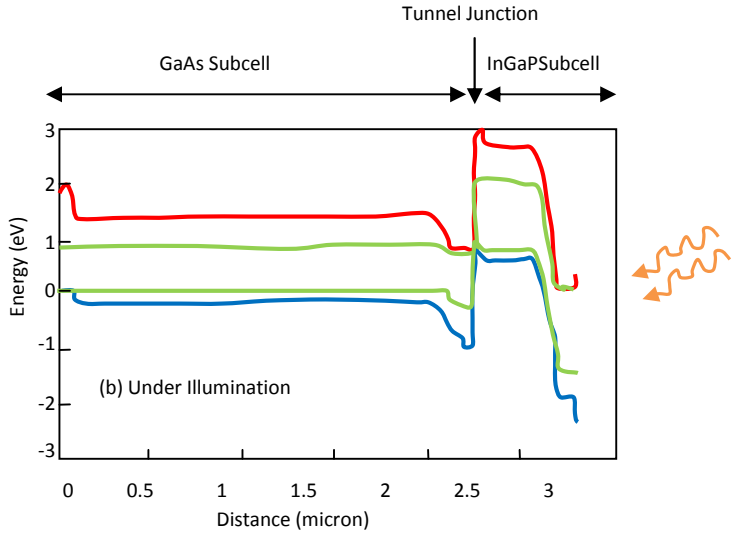

Figure 4.16 Band gap of 2J n+/p InGaP/GaAs solar cell (a) under equilibrium and (b) under illumination[30].

V_{oc} and V_m degrades when TDD increases in the 2J InGaP/GaAs solar cell on Si[56]as shown in Figure 4.17 (a). V_{oc} highly depends on the reverse saturation current density, J_{02}, associated with the depletion region recombination and that is the reason for the decrement in V_{oc}[12]. The V_{oc} can be expressed as,

$$V_{oc} = \frac{n_2 KT}{q} ln \frac{J_{sc}}{J_{o2}} \qquad (4.1)$$

where, J_{02} depends on the minority carrier base lifetime, τ_{base} and is expressed as,

$$J_{o2} = \frac{qn_i W_D}{2} \frac{1}{\tau_{base}} \qquad (4.2)$$

where, n_i is the intrinsic carrier concentration and W_D is the depletion layer width. The value of J_{02} increased at higher TDD because of reduction in minority electron lifetime[54]. Thus, the increase in J_0 led to significant degradation in both V_{oc} and V_m with increasing TDD.

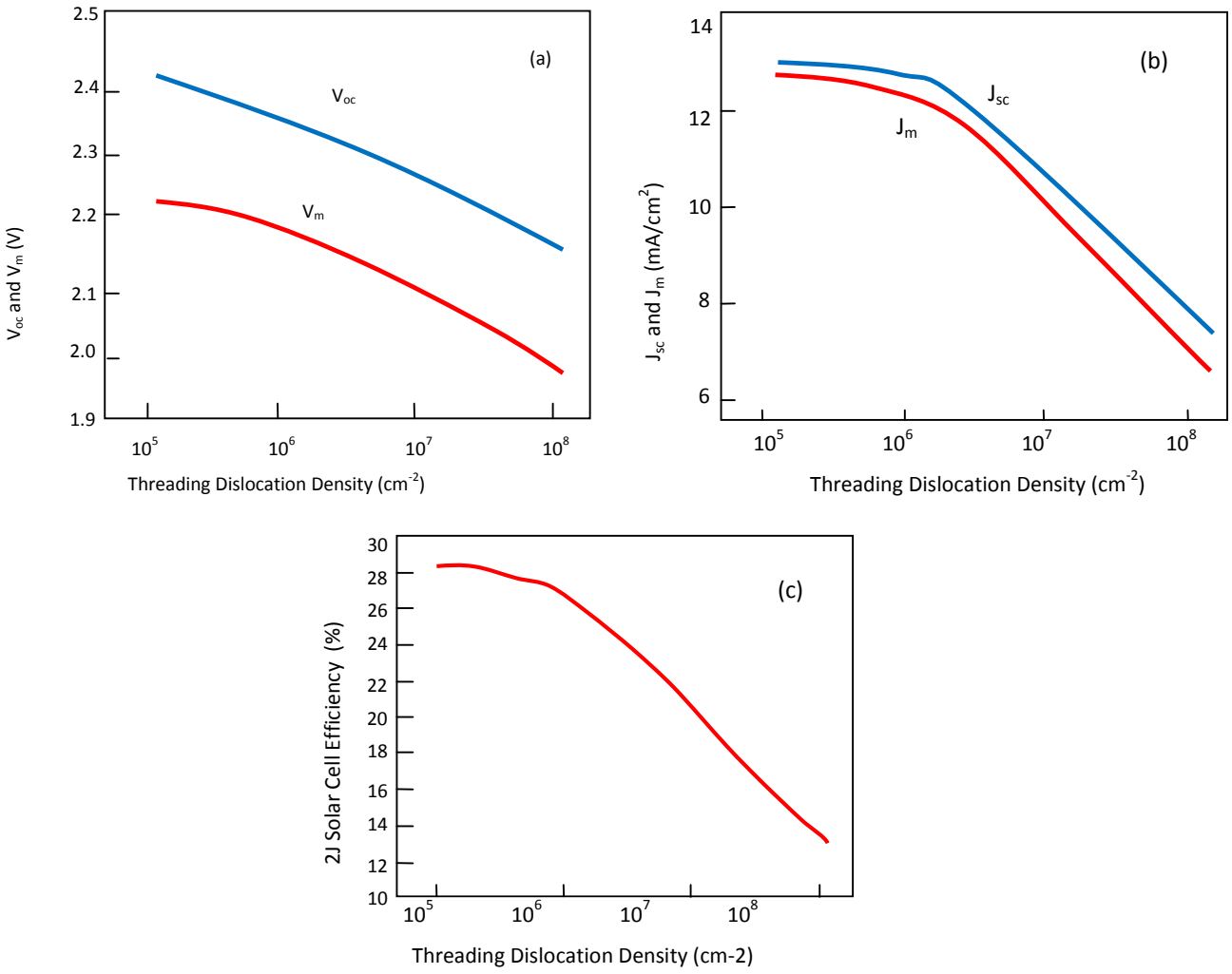

Figure 4.17 Impact of threading dislocation density variation on the performance of 2J InGaP/GaAs solar cell on Si: (a) Voc and Vm, (b) Jsc and Jm and (c) η under AM1.5G spectrum[56].

Figure 4.17 (b) shows J_{sc} and J_m in the 2J InGaP/GaAs solar cell on Si as a function of increase in TDD[56].The reduction of minority electron lifetime in GaAs and InGaP base led to degradation in J_{sc} and J_m at higher TDD. J_{sc} degradation occur at higher TDD than V_{oc} in 2J cell configuration, as same as 1J GaAs cell. Thus, J_{sc} was found to be more tolerant to TDD compared to V_{oc} for both 1J GaAs and 2J InGaP/GaAs cells on Si[54]. This clearly indicates that the performance of metamorphic solar cells was more impacted by the degradation in V_{oc} compared to the degradation in J_{sc}.

2J InGaP/GaAs cell efficiency decreases when TDD increases as shown in Figure 4.17 (c). The efficiency of this lattice-matched 2J InGaP/GaAs solar cell was about 28.5 and the efficiency at TDD of 10^6 $cm^{-2}$was 26.22%[12].The minority electron lifetime in the p-GaAs degraded beyond a TDD of 10^6 cm^{-2}[54]and affected the efficiency of the 2J InGaP/GaAs cell as the GaAs subcell was more sensitive to dislocations compared to InGaP. The 2J InGaP/GaAs solar cell efficiency degraded to that of 1J GaAs cell efficiency beyond a TDD of 10^7 cm^{-2}. Hence, TDD lower than 10^7 cm^{-2}shall be achieved in order to benefit from dual-junction cell design on Si.

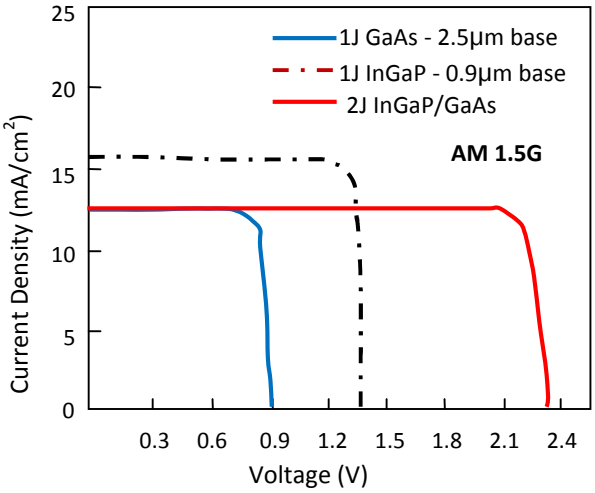

Figure 4.18 J-V characteristic of 2J cell along with the InGaP and GaAs subcell before current-matching at a TDD of 10^6 cm^{-2} at AM 1.5G[12].

Figure 4.18 shows the J-V characteristics of 2J InGaP/GaAs (red curve) cell, the GaAs subcell (blue curve) and the InGaP subcell (black curve) at a TDD of 10^6 cm^{-2}. The sub cells were not current-matched at the base thicknesses of 2.5µm and 0.9µm ofGaAs and InGaP respectively[12], and the bottom GaAs subcell limited the J_{sc} in the 2J cell configuration. It is challenging to improve the material quality of hetero-epitaxial GaAs grown on Si to lower the TDD significantly below 10^6 cm^{-2}. Hence, it is extremely important to optimize the metamorphic 2J InGaP/GaAs cell structure on Si at a realistic TDD of 10^6 cm^{-2} by tailoring the design of each subcell to realize the current-matching between them.

4.3.2.1 Current-Matching in Dual-Junction InGaP/GaAs Solar Cells on Si

In a multijunction cell, current-matching between the subcells is very important in order to get the best performance from a multi-junction cell[57]. The cell with a higher band-gap provides a

higher V_{oc} and lower J_{sc}. Ideally, J_m between each subcell should be matched to achieve the current-matching condition. Here, J_{sc} is used for current-matching as J_{sc} is a directly measurable parameter during cell characterization[56]and it has been widely used for current-matching analysis.

As shown in Figure 4.18, the sub cells of 2J solar cell design were not current-matched originally. Hence, design changes were required in order to achieve the current-matching condition between the subcells. In a solar cell, the thicker base layer absorbs most of the light and the minority carrier lifetime in the base has big role in determining the current density contribution from each sub cell[56]. Therefore, the base thicknesses in the GaAs and the InGaP subcells is optimized to achieve the current-matching condition at an experimentally realistic TDD of 10^6 cm^{-2}[55]. At this TDD, the value of τ_n calculated was as 1.494 ns and 3.171 ns in the p-GaAs and the p-InGaP base, respectively.

Figure 4.19 (a) shows 1J InGaP solar cell with the thickness of p-InGaP base varying from 0.3μm to 1.1μm. Then, the 2J cell with the thickness of p-InGaP base varied over the same range with the GaAs base thickness set to 1 μm (brown curve). The same procedure was repeated for the GaAs base thickness of 2 μm (black curve) and 3 μm (red curve)[58]. The InGaP solar cell structure was the same in both the 1J InGaP and the 2J InGaP/GaAs cell configurations. In 1J InGaP solar cell, J_{sc} decreases with thinning of the base thickness because of reduced absorption depth for the photons in the p-InGaP base. On the other hand, thinning the thickness of InGaP base in the 2J cell configuration let more photons to pass to the bottom GaAs sub cell and increases J_{sc} in the GaAs subcell at the cost of reduction in J_{sc} from the InGaP subcell[56]. This resulted in the overall increase in J_{sc} of 2J cell as the bottom GaAs subcell limited the J_{sc} in the 2J cell configuration. Thinning the top cell base while increasing the base thickness of the bottom GaAs subcell allowed additional photons through to the GaAs subcell and led to further improvement in the overall J_{sc} of the 2J cell. However, further increment in the GaAs base thickness beyond 2 μm didn't improve J_{sc} significantly due to insignificant photocurrent contribution from the GaAs subcell beyond a base thickness of 2 μm[58]. Hence, the minimal increase in J_{sc} by increasing the GaAs base thickness beyond 2 μm was related to inefficient carrier collection.

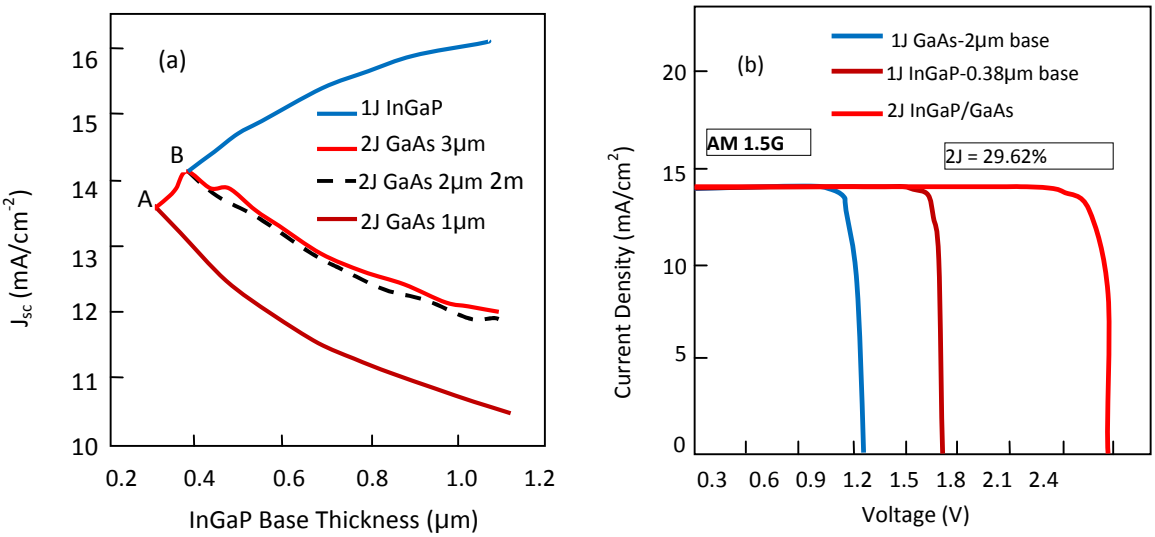

Figure 4.19 (a) Short-circuit current density as a function of top InGaP base, (b) Current-matched J-V characteristic in a 2JInGaP/GaAs solar cell at AM 1.5G[58].

The current-matching condition was attained at point A (J_{sc} = 13.5mA/cm^2) and B (J_{sc}=14.18 mA/cm^2) as shown in Figure 4.19 (a). The J-V characteristics of the 2J cell and the individual subcells corresponding to the point B were plotted in Figure 4.19 (b). At point B, the 2J cell exhibited a conversion efficiency of 29.62%[58]with a 2 µm and a 0.38 µm thick GaAs and InGaP base, respectively. Table 4.6 summarized the cell parameters before and after optimization at a TDD of 10^6 cm^{-2}. These results illustrate that even at a TDD of 10^6 cm^{-2}, an efficiency of greater than 29% can be realized for a metamorphic 2J InGaP/GaAs solar cell on Si by carefully engineering the cell design.

Table 4.6 Parameters for 2J InGaP/GaAs solar cell on Si: before and after optimization under AM1.5G [58].

2J InGaP/GaAs solar cell (base thickness in µm)	J_{sc} (mA/cm^2)	V_{oc}(V)	FF(%)	Efficiency (%)
Before optimization (0.9/2.5)	12.41	2.35	89.73	26.22
After optimization (0.38/2.0)	14.18	2.37	88.22	29.62

4.3.3 Triple-Junction InGaP/GaAs/Si Solar Cells on Si Substrate

The schematic of the 3J InGaP/GaAs/Si solar cell structure is shown in Fig 4.20[59]. A GaAs n-type buffer was selected to compliment the arsenic diffusion during the nucleation of III-V materials on the n-on-p Si solar cell.

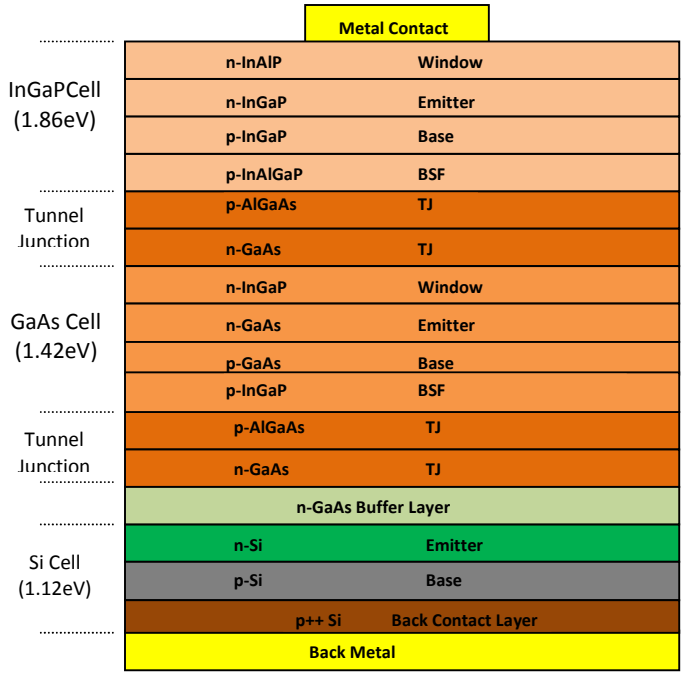

Figure 4.20Schematic depiction of tandem 3J InGaP/GaAs/Si solar cell employing Si active bottom cell[59].

4.3.3.1 Buffer Architecture for III-V-on-Si Integration

In the 3J InGaP/GaAs/Si solar cell, managing the light to reach the bottom Si sub-cell is a bit challenging[60] because of competition between the GaAs and Si sub-cell to absorb a shared regime of the incident solar spectrum[61]. Si has an indirect band-gap and needs a thicker layer to maximize absorption for current-matching with GaAs. GaAs is a direct band-gap material and requires thinner active cell layer compared to Si in order to absorb photons. In the 3J InGaP/GaAs/Si solar cell design, the indirect band-gap Si sub-cell was found to be the current-limiting one.

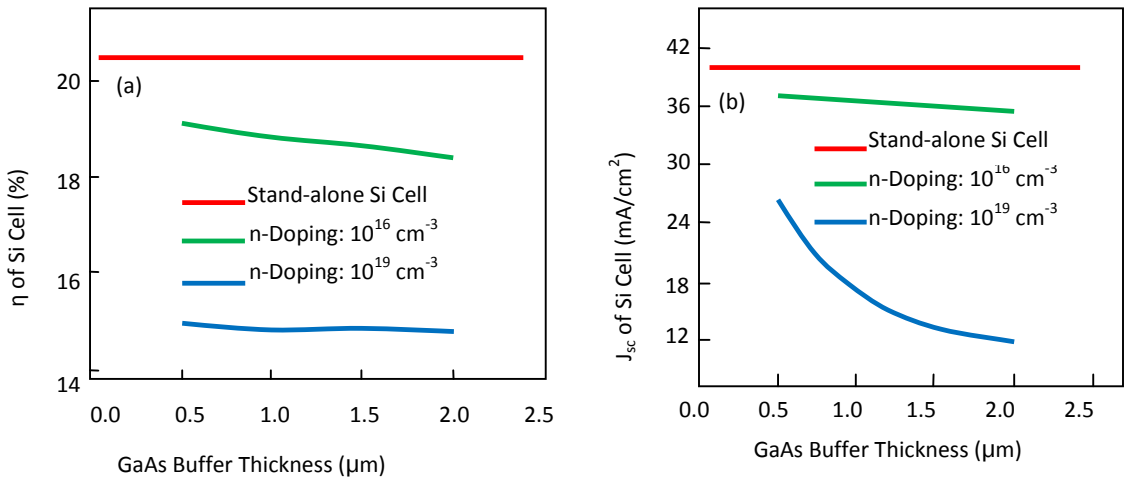

Figure 4.21 Impact of GaAs buffer thickness on 1J Si solar cell[60].

The efficiency and the short-circuit current density of the Si sub-cell for different GaAs buffer thicknesses (Fig. 4.21(a),(b)) and GaAs doping concentrations (Fig. 4.22(a),(b)) were evaluated[60].

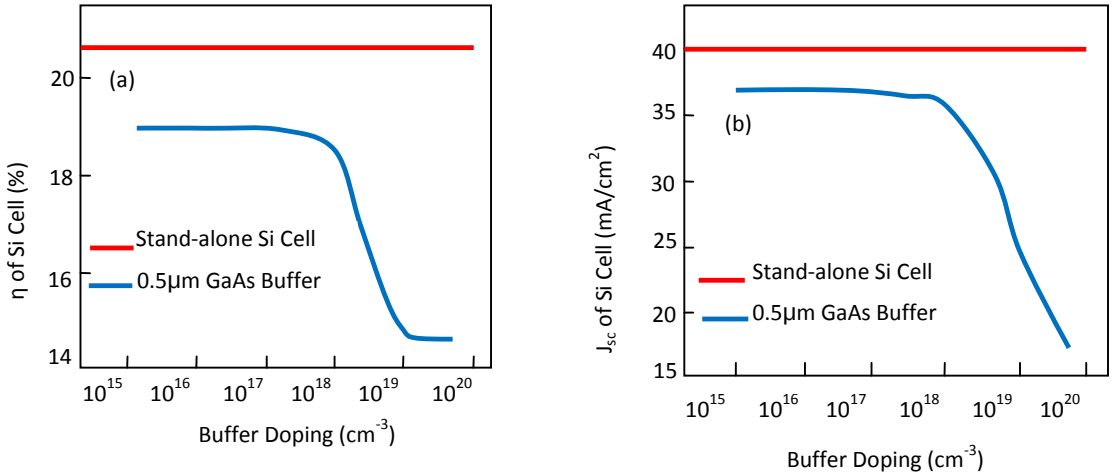

Figure 4.22 Impact of GaAs buffer doping on 1J Si solar cell [60].

The ideal stand-alone 1J Si solar cell efficiency was represented in red line in the above figures. The light penetration to the bottom Si sub-cell was lowered with increase in the GaAs buffer thickness and J_{sc} has decreased as shown in Fig. 4.21(b). In addition, the buffer thickness increment on the heavily doped GaAs buffer had a high impact on the Si sub-cell performance. The decrease in J_{sc} is associated to the decrease in Si cell performance (see Fig. 4.21(a)). The decrease in the J_{sc} was recognized as the key parameter degrading the Si sub-cell performance as the open-circuit voltage (V_{oc}) of the Si sub-cell reduced by less than 10% when the GaAs buffer

thickness was increased from 0.5µm to 2µm[60]. Thus, a thinner GaAs buffer would be preferable to maximize the Si sub-cell current response. Alternatively, materials with higher band-gap for buffer layer (such as InGaP and AlGaAs)[62], would relieve some of the constraint on the buffer layer thickness for III-V-on-Si integration.

Figure 4.22(a) showed the impact of GaAs buffer doping on the Si sub-cell performance at a buffer thickness of 0.5 µm. The heavily doped buffer had major impact on the performance of Si sub-cell due to narrowed band-gap in GaAs linked with the heavy doping effect[59]. Thus,the n-type GaAs buffer should have doping concentration less than $n=1x10^{18}cm^{-3}$ in order to allow light penetration to the bottom Si sub-cell.

4.3.3.2 Impact of Dislocations in the Buffer on Cell Performance

Figure 4.23 (a) and (b) showed the influence of GaAs buffer TDD on the 1J Si solar cell efficiency and the short-circuit current density[62]. The higher dislocation density in the GaAs buffer degraded the Si sub-cell performance as indicated in figure 4.23(a), because of poor minority hole transport across the n-type GaAs buffer[59]. So, current-matching 3J tandem cell configuration required high consideration on the dislocations in the GaAs buffer since it significantly affected light management and carrier collection.

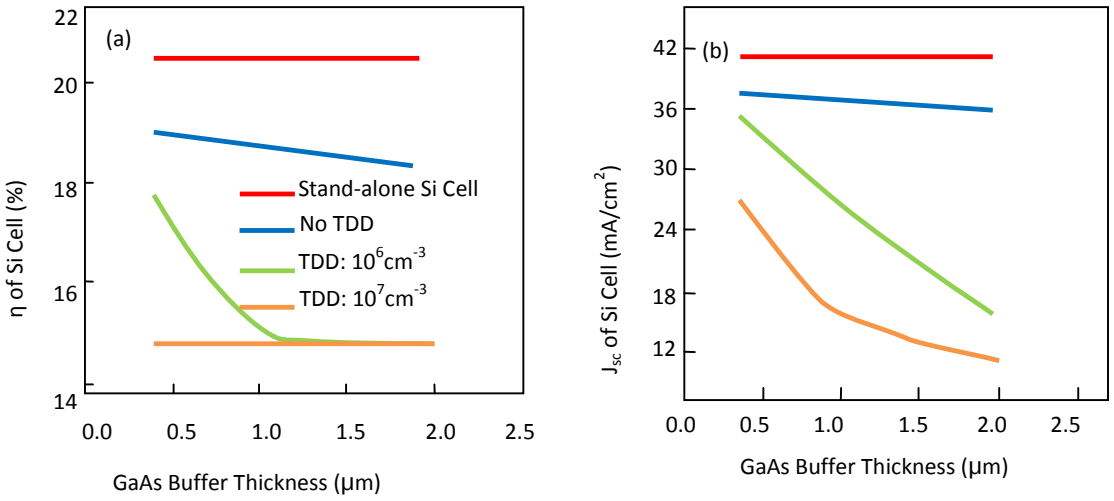

Figure 4.23 Impact of dislocation in GaAs buffer on 1J Si solar cell[62].

4.3.3.3 Triple Junction 1-Sun Design

The current-matching was challenging in the triple junction due to the propagated dislocations through the buffer layer into the active III-V layers[59]. The top InGaP and GaAs sub-cell

thicknesses should be reduced in order sufficient photon flux to reach the bottom Si cell. Moreover, thinning the III-V active cell layers let the minority carriers to travel shorter distance in the base to reach the junction and lowers the sensitivity of 3J III-V solar cell designs to TDDs. Based on GaAs buffer design optimization, 0.5µm thick GaAs buffer with a doping concentration of n=5x16 cm^{-3} were utilized to evaluate the performance of 3J InGaP/GaAs/Si tandem solar cells under 1-sun and CPV conditions [60].

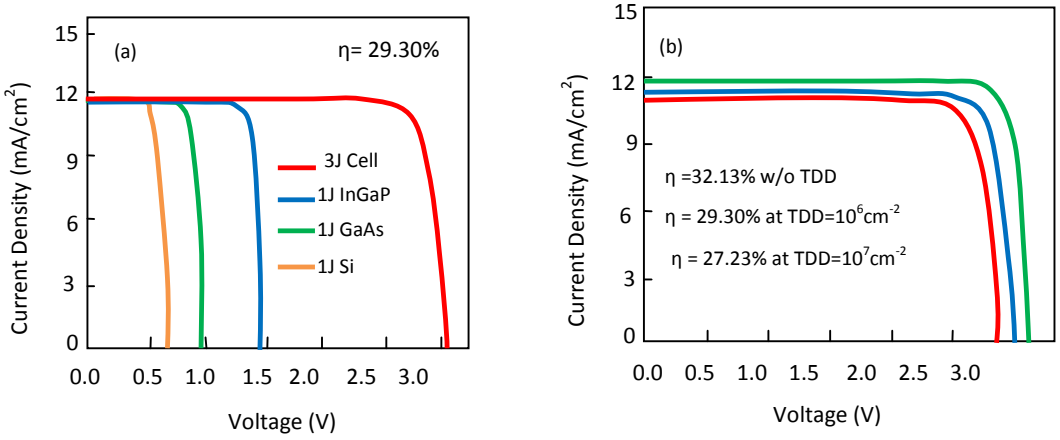

Figure 4.24 (a) Current-matched J-V curve for 3J InGaP/GaAs/Si cell at TDD=1x10^6 cm^{-2} (b) J-V curves for3J cell at different TDDs[60].

Fig. 4.24(a)shows the current-matched I-V characteristic of the 3J InGaP/GaAs/Si solar cell along with the I-V curves of the individual sub-cells at a realistic TDD of 10^6 cm^{-2}. The current-matched thickness of the top InGaP sub-cell (0.425 µm) and the middle GaAs sub-cell (0.87 µm) resulted in an efficiency of 29.30% (1-sun) under AM1.5d spectrum at a TDD of 10^6 cm^{-2}. The 3J design was also evaluated at a TDD of 10^7 cm^{-2} and exhibited an efficiency of 27.23% (AM1.5d) under current-matched condition, as shown in Fig. 4.24(b)[60]. The best-case scenario was also simulated when no buffer was present between the GaAs sub-cell and the Si sub-cell and entire cell stack was assumed to be free of dislocations. The Si sub-cell was connected to the top two III-V sub-cells by a GaAs/AlGaAs tunnel junction. The ideal case 3J design exhibited an efficiency of 32.13% under AM1.5d (1-sun). The 3J design was also evaluated under AM1.5g spectrum to compare the spectral differences. The thicknesses of the individual sub-cells were redesigned for current-matching, yielding an efficiency of 36.39% under AM1.5g (1-sun) as shown in Fig. 4.25. Table 4.8summarized the performance parameters for the 3J InGaP/GaAs/Si cell with TDD varied up to 10^7 cm^{-2}. It is noteworthy that even at a TDD of 10^7 cm^{-2}, careful current-matching enabled an efficiency of ~27% under 1-sun, emphasizing that such 3J III-V

solar cells utilizing the Si as a bottom sub-cell would be feasible and provide a promising path for extending single-junction Si solar cell performance. Such direct integration schemes are also of key interest for approaches involving mechanically stacking, transfer-printing and wafer-bonding of III-V solar cells with Si solar cell[59].

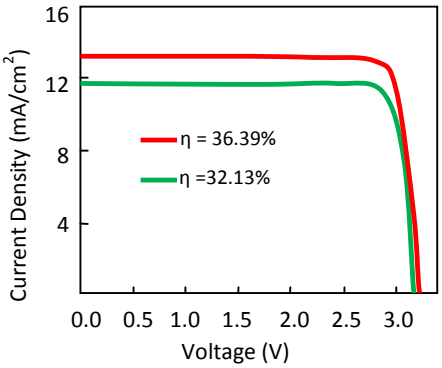

Figure 4.25 Comparison of current-matched J-V characteristic of 3J InGaP/GaAs/Si solar cells[60].

Table 4.7Performance dependence of 3J InGaP/GaAs/Si tandem solar cell on TDD at AM1.5d (1-sun) [60].

TDD	J_{sc}(mA/cm^2)	V_{oc}(V)	FF(%)	Efficiency (%)
No TDD	11.72	3.15	87.08	32.13
10^6	11.45	3.01	85.10	29.30
10^7	11.14	2.90	84.31	27.23

4.3.3.4 Triple Junction Concentrated Photovoltaic Design

The concentrated photovoltaic performance of the 3J InGaP/GaAs/Si solar cell at a realistic TDD density of 10^6 cm^{-2} was evaluated in [59]. In order to mitigate the losses due to shadowing effect and series resistance, the front grid-pitch was varied from 500 µm to 50 µm to evaluate the optimal grid design for CPV. A doping concentration of n=5x10^{18} cm^{-3} was utilized in the InAlP window layer to extend the peak performance towards higher sun concentration, as previously reported[63]. The solar cell performance parameters, namely efficiency, open-circuit voltage, fill-factor and peak voltage at maximum power point (V_m) are plotted as a function of

concentration in the Fig. 4.26(a), (b), (c) and (d), respectively. It can be clearly seen that with the reduction in the front grid-spacing, the 3J peak cell performance was extended to higher sun concentration. The design trade-offs between the losses due to the grid shadowing and the series resistance was best optimized at a grid-spacing of 200 μm, resulting in a conversion efficiency of 33.50% at 200 suns[59].

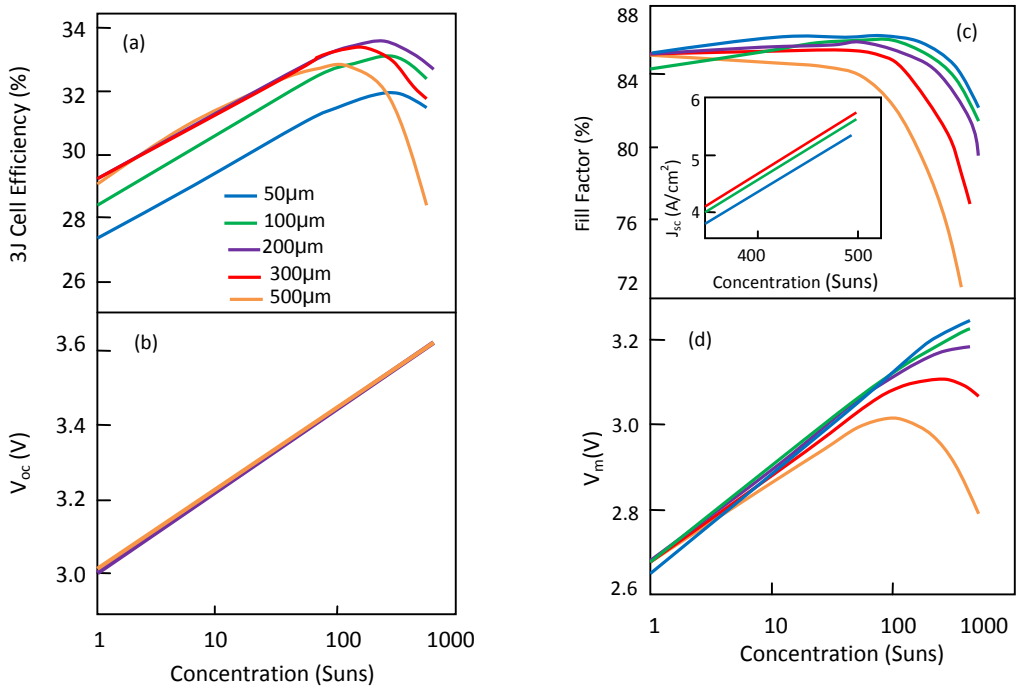

Fig. 4.26. CPV performance evaluation of 3J InGaP/GaAs/Si solar cell at a TDD of $1x10^6cm^{-2}$: (a) cell efficiency, (b) open-circuit voltage, (c) fill-factor and (d) peak voltage at maximum power point[59].

4.4 Comparison of III-V Solar Cells on GaAs, Ge and Si Substrate

Table 4.8 summarized the results obtained earlier for the III-V Solar Cells on GaAs, Ge and Si substrates and made a comparison among them. Open circuit voltage (V_{oc}), short circuit current (I_{sc}), fill factor (FF) and efficiency (η) were used to compare the performance of the solar cells. The fabrication technology, test condition and cost of solar cells were also considered for the comparison.

Table 4.8 Comparison of III-V Solar Cells on GaAs, Ge, Si Substrate

No	III-V Solar Cells	Condition	Dimension	V_{oc} (V)	I_{sc} (A/mm^2)	FF (%)	η (%)	Fabrication Technology	Cost	Year	Publisher	Remark
1.	**on GaAs Substrate**											
1.1	1Junction: GaAs	AM 1.5G, 1000W/m^2, 25^{0}c.	Anti reflective coating MgF_2/Zns:120nm/65nm GaInP Window: 30nm Emitter: 0.1µm	1.05	285	85.6	25	Epitaxial Growth	High	1990	Kurtz, et al.[44]	- AM: Air mass helps to define the length of the path through the atmosphere the radiation would have to travel in relation to the shortest length if the sun was in the apex AM = $1/\cos(Z)$ - AM1.5G (Global): on tilted surface with Zenith angle of 48^0. - Global: Direct + Diffuse radiation - In 1sun. (1sun = 1000W/m^2)
	1Junction: GaAs	AM 1.5G, 1000W/m^2, 25^{0}c.	Area: 0.9927cm^2	1.12	296.8	86.5	28.8	Thin Film	High	2013	Martin A. Green, et al.[5]	- GaAs active layer is used on GaAs substrate for lattice matched growth and better efficiency. - In 1 sun.
1.2	2Junction: InGaP/GaAs	AM 1.5G, 1000W/m^2, 25^{0}c.	Emitter: 50nm Base: 0.55µm Tunnel: 30nm	2.49	142.5	85.6	30.3	Epitaxial Growth	High	1997	Takamoto, T., et al.[49]	- Lattice Matched - In 1 sun.
	2Junction: InGaP/GaAs	AM 1.5G, 1000W/m^2, 25^{0}c.	Area: 4cm^2	2.488	142.2	85.6	30.3	Monolithic	High	2009	Green, M.A.; et al. [64]	- Lattice Matched - In 1 sun.

No	III-V Solar Cells	Result Condition	Size	V_{oc} (V)	I_{sc} (A/mm^2)	FF (%)	η (%)	Fabrication Technology	Cost	Year	Publisher	Remark
	2Junction: InGaP/GaAs	AM 1.5D, 1000KW/m^2, 25^{0}c.	-	-	-	-	32.6	Monolithic	High	2009	Garcia, et al.[51]	- Lattice Matched - In concentrated sun
	2Junction: InGaP/GaAs	AM 1.5G, 467KW/m^2, 25^{0}c.	-	-	-	-	34.1	-	High		NREL Website[6]	- Lattice Matched - In concentrated sun
2.	**on Ge Substrate**											
2.1	3Junction: InGaP/GaAs/Ge	AM 1.5G, 1000W/m^2, 25^{0}c.	-	2.62	143.7	85	32	Epitaxial Growth	High	2006	R.R. King, et al.[52]	- Lattice Matched - In 1 sun.
	3Junction: InGaP/GaAs/Ge	AM 1.5G, 240 kW/m^2, 25^{0}c.		2.91	159.6	87.5	40.7	Epitaxial Growth	High	2007	R.R. King, et al.[53]	- Metamorphic - In Concentrated sun
	3Junction: InGaP/GaAs/Ge	AM 1.5G, 454 kW/m^2, 25^{0}c.	-	-	-	-	41.1	Epitaxial Growth	High	2009	Guter, W., et al[65]	- In Concentrated sun
	InGaP/GaAs/InGaAs	AM 1.5G, 302kW/m^2, 25^{0}c.					44.4		High	2013	Martin A. Green, et al[5]	- Sharp, inverted metamorphic - In Concentrated sun
3.	**on Si Substrate**											
3.1	1Junction: GaAs	AM 1.5, 1000W/m^2, 25^{0}c.	7 µm GaAs buffer	0.89	255	77.7	17.6		Low	1988	Spire / NREL[66]	- In 1 sun
	1Junction: GaAs	AM 1.5G, 1000W/m^2, 25^{0}c.	10 µmSiGe buffer	0.97	238	78.1	18.1		Low	2005	Ohio State University[67]	- In 1 sun
	1Junction: GaAs	AM 0, 1000W/m^2, 25^{0}c.		0.94	332	79.1	18.3		Low	1988	NTT Japan[68]	Strained-layer superlattice& GaAs/AlGaAs buffer - In 1 sun
	1Junction: GaAs	AM 1.5G, 1000W/m^2, 25^{0}c.	-	-	-	-	20		Low	1988	NTT Japan[68]	Strained-layer superlattice& GaAs/AlGaAs buffer. In 1 sun.

No	III-V Solar Cells	Result Condition	Size	V_{oc} (V)	I_{sc} (A/mm^2)	FF (%)	η (%)	Fabrication Technology	Cost	Year	Publisher	Remark
	1Junction: GaAs	AM 1.5GD, 200KW/m^2, 25^{0}c.	-	-	-	-	21.3		Low	1991	Spire / NREL[69]	- GaAs Buffer. -In concentrated sun.
	1Junction: GaAs	AM 1.5G 1000W/m^2, 25^{0}c.	Base Thickness: GaAs - 2.5µm	1.05	290	87	26	Epitaxial Growth	Low	2013	Nikhil Jain[12]	- TDD 10^4cm^{-2} TDD: Threading Dislocation Density - In 1 sun.
3.2	2Junction: InGaP/GaAs	AM 1.5G 1000W/m^2, 25^{0}c.		1.94	112	75.3	16.4		Low	2014	FraunhoferISE[70]	- GaAsP buffer - In 1 sun.
	2Junction: InGaP/GaAs	AM 1.5G 1000W/m^2, 25^{0}c.		2.18	105	75.3	16.8		Low	2006	Ohio State University[71]	- SiGe buffer - In 1 sun.
	2Junction: InGaP/SiGe	AM 1.5G 1000W/m^2, 25^{0}c.		1.45	181	72	18.9		Low	2014	Multiple[72]	- SiGe buffer - Under 1 sun condition.
	2Junction: IAlGaAs/Si	AM 0, 1000W/m^2, 25^{0}c.		1.57	236	77.2	21.2		Low	1997	Nagoya Institute [73]	- GaAs/AlGaAs buffer - Under 1 sun condition.
	2Junction: InGaP/GaAs			1.55	279	58	25.2	Waffer bonding	Low	2012	University of Tokyo [74]	- Under 1 sun condition.
	2Junction: InGaP/GaAs	AM 1.5G 1000W/m^2, 25^{0}c.		2.39	127	85.9	26	Waffer bonding	Low	2014	FraunhoferISE[70]	- Under 1 sun condition.
	2Junction: InGaP/GaAs	AM 1.5G 1000W/m^2, 25^{0}c.	Base Thickness: InGaP - 0.9µm GaAs - 2.5µm	2.34	128	-	28.5	Epitaxial Growth	Low	2013	Nikhil Jain[12]	- TDD 10^4cm^{-2} -Lattice Matched - Under 1 sun condition.

No	III-V Solar Cells	Result Condition	Size	V_{oc} (V)	I_{sc} (A/mm^2)	FF (%)	η (%)	Fabrication Technology	Cost	Year	Publisher	Remark
	2Junction: InGaP/GaAs	AM 1.5G 1000W/m^2, 25^0c.	Base Thickness: InGaP - 0.38µm GaAs - 2µm	2.37	141.8	88.2	29.62	Epitaxial Growth	Low	2013	Nikhil Jain[12]	- TDD 10^6cm^{-2} -Metamorphic and optimized with current matching. - Under 1 sun condition.
3.3	3Junction:	AM 1.5G, 1000W/m^2, 25^0c.		2.74	118	79	25.5	Direct metal interconnect	Low	2014	McMaster University[75]	- Under 1 sun condition.
	3Junction:	AM 1.5D, 1000W/m^2, 25^0c.		2.78	856	86.3	20.5	Wafer-bonding	Low	2008	FraunhoferISE[76,77]	- Under 1 sun condition.
	3Junction:	AM 1.5D, 48KW/m^2, 25^0c.		3.33	614	82.9	27.9	Wafer-bonding	Low	2008	FraunhoferISE[76,77]	- Under concentrated sun
	3Junction: InGaP/GaAs/Si (TDD 10^6cm^{-2})	AM 1.5G, 1000W/m^2, 25^0c.	Base Thickness: InGaP - 0.38µm GaAs - 2µm Buffer Thickness: GaAs - 0.5µm	3.01	114.5	85.1	29.3	Epitaxial Growth	Low	2015	Nikhil Jain[62]	- TDD 10^6cm^{-2} - Under 1 sun condition.
	3Junction: InGaP/GaAs/Si (TDD 10^6cm^{-2})	AM 1.5G, 200kW/m^2, 25^0c.	Grid spacing: 200µm	3.5	~200	85	33.5	Epitaxial Growth	Low	2015	Nikhil Jain[62]	- TDD 10^6cm^{-2} - Under concentrated sun

The performances of III-V Solar cells on GaAs substrate were shown in Table 4.8, item No.1. For this substrate, single Junction and dual junction solar cell configurations were applied. GaAs was used for the active layer of a single junction and for the bottom layer of dual junction in order to have a lattice matched arrangement with the GaAs substrate and to maximize the solar cell efficiency. InGaP compound is lattice matched with GaAs compound with a proper composition and was used for the upper active layer of a dual solar cell configuration. Accordingly, the latest efficiency achieved for a single Junction III-V Solar cell on GaAs substrate with thin film fabrication technology was 28.8%[5]in 1sun (1000W/m^2) at AM 1.5G, 25^0c and the latest efficiency achieved for a dual Junction III-V Solar cell of InGaP/GaAs on GaAs substrate was 34.1%[6] at concentrated sun of 467KW/m^2at AM 1.5G, 25^0c.

Secondly, the performance of triple Junction Solar cell on Ge substrate was shown in Table 4.8. Ge is nearly lattice matched with GaAs and a small amount of In to GaAs allow exact lattice matching to Ge substrates. So, Ge is usually used in triple designs as substrate and the lowest bandgap component. The recent conversion efficiency of a triple Junction III-V Solar cell of InGaP/GaAs/InGaAs on Ge substrate with sharp inverted metamorphic technology was 44.4%[5] at concentrated sun of 302KW/m^2 at AM 1.5G 25^0c.

The high cost of III-V solar cells has limited their application and lowering the cost by substituting the substrate with Si material is a good option based on a recent study that revealed transitioning of a 4” Ge or GaAs substrate to 8” Si substrate would correlate to about 60% reduction in cost for multijunction solar cells[78]. Following that, Table 4.8 showed the conversion efficiencies of single, dual and Triple III-V solar cells on Si substrate. The latest efficiency achieved for a single Junction III-V Solar cell of GaAs on Si substrate with epitaxial growth fabrication and TDD of $10^4cm^{-2}$was 26%[12] in 1sun (1000W/m^2) at AM 1.5G, 25^0c, the recent efficiency of a dual Junction III-V Solar cell of InGaP/GaAs on Si substrate with epitaxial growth fabrication and TDD of $10^6cm^{-2}$was 29.62%[12]in 1sunat AM 1.5G, 25^0c and the recent efficiency of a triple Junction III-V Solar cell of InGaP/GaAs/Si on Si substrate with epitaxial growth fabrication and TDD of $10^6cm^{-2}$was 33.5%[62] in concentrated sun of 200KW/m^2at AM 1.5G, 25^0c.

Based on the review, the highest efficiency achieved for 1J GaAs cell on Si substrate with Base thickness of 2.5µm, TDD $10^4 cm^{-2}$ was 26%[12] in 1sun ($1000W/m^2$), while the record efficiency for GaAs solar cell on GaAs substrate was 28.8%[5] in 1sun ($1000W/m^2$). The efficiency of optimized metamorphic 2J InGaP/GaAs solar cell on Si substrate with Base thickness of 0.38µm (InGaP), 2µm (GaAs), TDD $10^6 cm^{-2}$ is about 29.62%[12] in 1sun, while the record efficiency for 2J InGaP/GaAs cells on GaAs substrate is about 34.1%[6] in 467sun. The efficiency of the 3J InGaP/GaAs/Si solar cell on Si substrate at a realistic TDD density of 10^6 cm^{-2} was 33.50%[62] in 200 suns, while the highest efficiency achieved for InGaP/GaAs/Ge solar cell on Ge substrate is 44.4%[5] in 302 sun.

CHAPTER 5

CONCLUSION AND RECOMMENDATION

5.1 Conclusion

The III-V compound based semiconductor multijunction solar cells have been the most successful technology for delivering the highest photovoltaic conversion efficiency. However, their expensive cost has limited their applications. III-V solar cells performance is increasing every year but the low cost silicon solar cell made it challenging for high efficiency III-V solar cells to make a strong commercial impact.

In this thesis, the performance of 1Junction GaAs on GaAs substrate, 2Junction InGaP/GaAs on GaAs substrate, 3Junction InGaP/GaAs/Ge, InGaP/GaAs/InGaAs on Ge substrate, 1Junction GaAs on Si substrate, 2Junction InGaP/GaAs on Si substrate, and 3JunctionInGaP/GaAs/Si solar cells on Si substrate have been comprehensively investigated.

Based on the study, the efficiencies of 1-Junction and 2-Juntion III-V Semiconductor Solar cells on Si substrate are increasing per year approaching the Solar cell on GaAs substrate. The study showed that the successful integration of III-V solar cells on Si substrate is very promising to lower the cost of solar energy by merging the high efficiency III-V materials with the low-cost and abundant Si substrate.

5.2 Recommendation for Future Work

The research showed that the efficiency of 3-Junction III-V solar cell (InGaP/GaAs/Si) on Si substrate is low compared to 3Junction InGaP/GaAs/Ge, InGaP/GaAs/InGaAs on Ge substrate and more work shall be done to achieve higher efficiency for 3Junction III-V Solar cells on Si substrate. In addition it's recommended to review the performance of 4 and more Junction III-V solar cells on Si substrate in order to exploit the excellent energy conversion properties of III-V semiconductors with the volume manufacturability of Si substrate.

APPENDIX A

FABRICATION OF III-V SOLAR CELLS

There are generally two ways to realize a multi-junction solar cell, either mechanically or monolithically. Mechanically stacked multijunction solar cells consist of multiple single-junctions of different materials manufactured on separate substrates, and then stacked on top of each other, with multiple sets of terminals; while monolithically stacked multi-junction solar cells have a series of junctions directly grown on one substrate, and interconnected by tunnel junctions in series. As a result, there are only two terminals.

During the early development, best results were obtained for the mechanically stacked solar cells[79]. Later on, the rapid advance in metal organic vapor phase epitaxy MOVPE technology triggered an increased interest in the monolithically stacked multi-junction solar cell. MOVPE is named after the metal organic compounds that are used as precursors for the metallic group-III elements. The metal-organic compounds are mixed with precursors containing a group-V element during the epitaxial growth. Especially, the growth of dual-junction $Ga_{0.5}In_{0.5}P/Ga_{0.99}In_{0.01}As$ cells on germanium substrates and the later state-of-the-art triple-junction $Ga_{0.5}In_{0.5}P/Ga_{0.99}In_{0.01}As/Ge$ device structures continuously pushed the performance of the monolithic stack higher. The monolithic integration circumvents the additional optical loss and complexity of mechanical stacking. Moreover, only one substrate is needed, in contrast to the other mechanical stack designs at that time, which include two substrates.

However, the monolithic design is not without limitations. Since the junctions are grown directly in contact and series-connected by tunnel junctions, lattice matching and current matching are required. In fact, the complexity of stacking multiple junctions lies in the MOVPE cell material growth, and the difficulties in growth increase super-linearly with the number of junctions in the stack. More importantly, when monolithic designs with more junctions (4 junctions and above) are pursued, the current matching requirement and resulting spectral sensitivity problem will greatly compromise the yearly energy yield, even if a higher efficiency is obtained for a certain reference spectrum.

During the past years, wafer bonding technologies have become an important process in the fabrication of both microelectronic systems and micro electromechanical systems (MEMS). It

enables fabrication and packaging of complex three dimensional micro components (i.e. 3D stacked IC's)[80]. These same bonding technologies and related expertise can be transferred and applied to mechanically stacking solar cell device wafers, tackling the processing complexity. Together with improved designs, the performance can be further improved and the cost can be reduced.

A.1. Mechanical Stacking

Since mechanically stacked solar cells are electrically separated, normally they are processed on different substrates and have multiple terminals instead of two[79]. To reduce the cost and bulkiness of the mechanical stack, a single-substrate design is proposed, with thin film III-V cells consisting of only the active absorber layer and supported by a substrate based bottom cell.

In essence, each III-V sub-cell is still grown on separate substrates and processed individually. Subsequently, the thin active layer is released from its substrate and stacked on the wafer-based bottom cell. In principle, the Ge or GaAs substrates for MOVPE growth can be reused again after proper cleaning and preconditioning. In current study, the well-known InGaP, GaAs and Ge junctions are used for the development of the triple-junction stack, and the III-V solar cells are grown on germanium substrates. Extra optical losses are unavoidable; however they can be kept at the minimum. Transparent adhesive layers are used to bond sub-cells together, and ARC layers are introduced at each cell surface to reduce reflection losses. All ARC layers are optimized simultaneously for the whole multi-junction stack, taking into account the differences in cell performance. Metal grids throughout the stack have the same pattern design and are accurately aligned, avoiding extra shadowing. It is worth to mention that the stacking of upper III-V cells is very generic and repeatable[79]. The stacking of top InGaP junction can be realized in a similar manner as the thin GaAs junction, with little or no changes.

The developed process flow of mechanically stacked multi-junction solar cells basically involves a thin layer transfer process, releasing the active III-V layer from its original growth substrate and stacking onto the underlying supporting bottom cell.

After MOVPE growth and front side metallization, the GaAs solar cell device wafer is temporarily bonded to a carrier by adhesive bonding. The carrier wafer then provides necessary mechanical support during the substrate removal and further backside processing for the thinned

down GaAs cells. Eventually, the thin GaAs cell layer is transferred to a separate fully processed Ge bottom cell device wafer by permanent adhesive bonding, and the temporary carrier can be released.

At this stage, a GaAs-Ge dual-junction mechanical stack is formed. By repeating the same process again for the InGaP junction, InGaP-GaAs-Ge triple-junction mechanical stacks can be realized.

The successful development of a few key processing steps, such as void free wafer bonding, thin wafer handling and compatible backside processing for the III-V cells, proves to be crucial for the development of the mechanical stack process. Moreover, it is worth to mention that the developed layer transfer process is fully wafer-level processing, which enables this technology in a potential high-volume production environment. In addition, due to its similarities with 3D stacking of IC's, it can largely benefit from the rapidly emerging field of 3D integration.

A.2. Growing Methods

Growing methods for III-V solar cells can be divided in to two categories: bulk growth methods as Czochralski and Bridgman methods, or epitaxial growth methods[28]. The main methods are described below for the growth of GaAs, being this the most important compound of the group; all the other compounds, including ternary and quaternary compounds, are grown using the same techniques, and adding the necessary elements, Al, In, Sb, etc. in the required proportions.

A.2.1. Bulk growth

The Czochralski method grows the compound from the molten. A seed, with the desired crystalline structure is put in contact with the molten, and pulled out slowly enough for a crystal to grow on the seed. The boule is rotated to favor uniformity in temperature and compound density. The transition from the liquid phase to the crystalline phase ensures a purification of the residual impurities in the molten in agreement with their segregation coefficients[34,13]. This is the main method used to grow silicon crystals.

The Czochralski method for growing single crystals of GaAs must be modified due to the volatility of As at Ga melting point temperature (1238^{o}C). So, the molten is covered with a 1 cm thick layer of boron trioxide B_2O_3 which, in conjunction with high pressure inert gas in the growing chamber prevents the evaporation of As. This method is known as Liquid Encapsulated Czochralski(LEC) method. Doping elements or other III-V elements required for growing

ternary or quaternary compounds can be added to the molten in order to obtain the desired proportion of elements in the compound.

Bridgman method is a two-zone technique, where a crucible of graphite is pulled from one side of a sealed tube made of quartz, at a temperature of 1242-1460^{o}C, above Ga melting point, to the other side with a temperature of 610-620^{o}C, to maintain the necessary overpressure of As. A seed of GaAs is set at the coolest edge of the crucible to establish the crystal orientation.

A.2.2 Epitaxial growth

The most efficient III-V solar cells are manufactured based on epitaxial growth methods. Epitaxy consists the ordered growth of one crystal upon another, whose orientations are related and well defined[28]. It could be a homo-epitaxy, when growing a new layer of the same compound on top of the substrate, or hetero-epitaxy, when the compound grown is different from the substrate. In the case of III-V semiconductors these techniques allow for a wide range of electronic and optoelectronic properties influenced by the substrate. The introduction of ternary and quaternary compounds, as for example Al_xGa_{1-x}Asand $In_xGa_{1-x}As_yP_{1-y}$, offers even further possibilities. Even in the case of lattice mismatch, elastic strained structures can be produced by slowly modifying the relative proportions of the elements of the compound. This can be achieved due to the low growing rates of epitaxial techniques which allows for flexibility in the selection of the semiconductors used, its thickness, as well as the type and profile of the doping (due to the low temperature used in this methods the cross-diffusion of dopants and impurities is very reduced). Control over the growing process to one monolayer level offers the possibility of growing layered structures, known as superlattices, where layers of different compounds are grown upon each other with a thickness smaller than electronic mean-free path. All this allows for high purity compounds with high values of mobility, life-time and mean-free path for minority carriers.

A.2.2.1. Liquid Phase Epitaxy (LPE)

This method deposits epitaxial layers from the liquid phase materials, and takes advantage of the fact that adding impurities to the molten reduces the melting point temperature (e.g. GaAs +As melting point is lower than that for GaAs), and therefore the molten can be kept to a lower temperature such that the seed will not melt[28]. The solution is cooled slowly and new epitaxial layers form on the seed of GaAs. Since the concentration of impurities in the liquid solution increases as the crystal grows it is necessary to further reduce temperature to continue the

growing process. Therefore, the epitaxial growth is controlled by the rate at which temperature is lowered. By growing the crystal from the liquid state the segregation of impurities ensures the high purity of the crystal.

A.2.2.2 Chemical Vapor Deposition (CVD)

CVD is also known as Vapor Phase Epitaxy (VPE) and grows crystals form gaseous Ga and As compounds, which react on a substrate to form GaAs at temperatures of about 650-850^{o}C [34,13]. The whole process comprises several steps, first the reactants (gases and dopants) are transported to the substrate, then are transferred and absorbed into the substrate, where the chemical reaction catalyzed at the surface takes place and the layer is grown at rates of 1µm/h. Finally, the gaseous sub products are desorbed to the gas stream and transported out of the reaction chamber. In the most elemental reaction $GaCl_3$ and As_4 are transported to the substrate with hydrogen H_2, producing the reaction:

$$GaCl_3 + As + 6H_2 \rightarrow 4GaAs + 12HCl \qquad (A.1)$$

A.2.2.3. Metal Organic Chemical Vapor Deposition (MOCVD)

MOCVD is a particular kind of CVD growth process characterized by the chemical nature of the precursors. Metal-organic compounds with relatively high volatility are used as precursors for both, main elements and doping elements. In this case trimethyl-gallium (TMGa) and arsine are carried by hydrogen at atmospheric pressure to the substrate, which is heated at 600-800^{o}C by radio frequency (RF) to produce the pyrolitic reaction [16]:

$$Ga(CH_3)_3 + AsH_3 \rightarrow GaAs + 3CH_4 \qquad (A.2)$$

A.2.2.4. Molecular Beam Epitaxy (MBE)

MBE is a technique where a reaction of thermal gaseous beams of molecules from evaporation or sublimation of liquids or solids with a crystalline surface is produced under ultra-high-vacuum conditions to form the epitaxial layer[13]. This vacuum conditions together with the highest standards of cleanness used in the construction of the techniques and apparatus allows for a high purity of the grown samples.

The reactants are evaporated from separated graphite effusion ovens (Knudsen cells), heated radiatively to the convenient temperature to adjust the evaporation rate (in particular an

overpressure of As_4 is maintained to compensate its low sticking coefficient). To ensure the uniformity of the layers the substrate rotates once per monolayer grown[81,82]. The growth rate of this technique is lower than for MOCVD (< 1µm/h). The ability to stop and start the beams in a shorter time than required for growing a layer allows for monolayer precision and unique doping profile in the growing process.

When molecular organic compounds are used the method is called Molecular Organic MBE (MOMBE, also known as Chemical Beam Epitaxy, CBE). This allows for a uniform source flux over a large area[83]. In the Gas Source MBE (GSMBE) gases are changed from outside the ultra-high-vacuum chamber, which makes the process more flexible.

References

[1] Central Statistical Agency (CSA) "Population Size", 2014

[2] Paul Hersch, Kenneth Zweibel, "Basic Photovoltaic Principles and Methods" by Solar Energy Research Institute, Colorado, February 1982

[3] Bailey, Robert L., "Solar Electrics Research and Development" Ann Arbor, MI: Ann Arbor Sciences , pp. 2-186, 1980

[4] Dickinson, William C, "Solar Energy Technology Handbook, Part A" New York, NY: Marcel Dekker, Inc.; pp 1-167, 1980

[5] M. A. Green et al., "Solar cell efficiency tables (version 42)," Progress in Photovoltaic: Research and Applications, vol. 21, 2013, pp. 1.

[6] http://www.nrel.gov/ncpv/, National Renewable Energy Laboratory, retrieved in January 2016.

[7] http://www.greenrhinoenergy.com/solar/radiation/spectra.php, Greenrhino Energy, retrieved in January 2016

[8] C. L. Andre, A. J. Pitera " Photovoltaic Devices: Solar cells", pp. 520, 2006.

[9] M.A. Green, "Solar Cells: Operating principles, technology, and system applications", New Jersey: Prentice Hall 1982.

[10] W. Shockley “Electrons and Holes in Semiconductors”, D. Van Nostrand, Princeton, N.J., 1950.

[11] Jenny Nelson The Physics of Solar Cells, Imperial College Press, 2003.

[12] Nikhil Jain, "Design of III-V Multijunction Solar Cells On Silicon Substrate" in Thesis submitted to the faculty of the Virginia Polytechnic Institute and State University, May 2013.

[13] S. M. Sze, Semiconductor Devices, Physics and Technology, (John Wiley & Sons, 1985).

[14]Ottfried Madelung Semiconductors: Data Handbook, 3rd edition Springer (2004).

[15]T.P.Pearsall, GaInAsP Alloy Semiconductors, John Wiley and Sons (1982).

[16] R. A. Stradling and P. C. Klipstein, Growth and Characterization of semiconductors, (Adam Hilger, Bristol and New York,1990).

[17] N.V. Yastrebova et al., "High-efficiency multijunction solar cells: Current status and future potential," University of Ottawa, 2007.

[18] Green, M.A.; Emery, K.; Hishikawa, Y.; Warta, W. Solar cell efficiency tables (version33). Prog. Photovoltaics Res. Appl. **2009**, 17, 85–94.

[19]Katsuaki Tanabe, "A Review of Ultrahigh Efficiency III-V Semiconductor Compound Solar Cells: Multijunction Tandem, Lower Dimensional, Photonic Up/Down Conversion and PlasmonicNanometallic Structures", by Institute of Industrial Science, University of Tokyo, 2009.

[20]D.E.Aspnes, Phys. Rev., B14, no.12, pp.5331-5343 (1976)

[21] P Bhattacharya, Semicond. Sci.Technol. 3 pp. 1145-1156 (1988).

[22]Sadao Adachi (Ed.), Properties of Aluminum Gallium Arsenide, EMIS data reviews series no. 7, INSPEC (1993).

[23] V. M. Andreev, V. P. Khvostikov, V. R. Larionov, V. D. Rumyantsev, E. V. Paleeva, M. Z. Shvarts, SEMICONDUCTORS, Vol. 33, 9, p. 976 (1999).

[24] Wei Zhang, Mengyan Zhang, Mingbo Chen, Depeng Jiang, Liangxing Wang, Proc. ISES WORLD CONGRESS 2007 (VOL. I – VOL. V), 4, 996-999 (2009).

[25] D.J. Friedman*, J.F. Geisz, S.R. Kurtz, J.M. Olson, Journal of Crystal Growth 195 (1998) 409—415

[26] J F Geisz and D J Friedman, Semicond. Sci. Technol. 17 (2002) 769–777

[27]VijitSabnis, Homan Yuen, and Mike Wiemer, 7th international conference on concentrating photovoltaic systems CPV7 in press (2012)

[28] Jose Maria Roman, "State-of-the-art of III-V Solar Cell Fabrication Technologies, Device Designs and Applications", Advanced Photovoltaic Cell Design EN548, April, 2004.

[29] VM Andreev, “GaAs and High-Efficiency Space Cells” in “Practical handbook of photovoltaic: fundamentals and applications”, Eds. T. Markvart and Luis Castañer, Elsevier, (2003).

[30] N. Jain and M.K. Hudait, "Impact of Threading Dislocations on the Design of GaAs and InGaP/GaAs Solar Cells on Si Using Finite Element Analysis, " IEEE Journal of Photovoltaic, vol. 3, 2013, pp. 528.

[31] M. Y. Ghannam, et al., "Theoretical study of the impact of bulk and interface recombination on the performance of GaInP/GaAs/Ge triple junction tandem solar cells," in Proc. 3rd World Conf Photovoltaic Energy Convers., 2003

[32]F.Himrane, N.M. Pearsall, R.Hill, IN: IEEE Photovoltaic Specialists Conference, 18th, Las Vegas, NV, October 21-25, 1985, Conference Record (A87- 19826 07-44). New York, Institute of Electrical and Electronics Engineers, Inc., p. 338-343 (1985).

[33] Pearsall, T.P. Ed. Properties, Processing and Applications of Indium Phosphide, IEE/INSPEC, The Institution of Electrical Engineers, London, (2000).

[34] Richard H. Bube, Photovoltaic Materials, (Imperial College Press, 1998).

[35] S. M. Hubbard, C. D. Cress, C. G. Bailey, R. P. Raffaelle, S. G. Bailey, and D.M. Wilt, Appl. Phys. Lett. 92, 123512 (2008).

[36] Alex Trellakis · Tobias Zibold · Till Andlauer · Stefan Birner · R. Kent Smith Richard Morschl · Peter Vogl, J Comput Electron 5:285–289 (2006).

[37]] James P. Connolly, Denis Mencaraglia, III-V Solar Cells, Nanophotonic Technology Centre, Universidad Politécnica de Valencia, Camino de Vera s/n, 46022 Valencia , Spain (2012).

[38] S. M. Sze and Kwok K. Ng, Physics of Semiconductor Devices, (7th edition, John Wiley & Sons, 2007).

[39] Matthias E. Nell and Allen M. Barnett, IEEE Trans. Elect. Devices, Vol ED-34, No. 2, 1987.

[40]W.Shockley and W.T.Read, Phys. Rev. 87 (1952) 835, and R.N.Hall, Phys. Rev. 87, 387. (1952).

[41] G. L. Araujo and A. Marti, Sol. Energy Mater. Sol. Cells 33, 213, 1994.

[42] Jenny Nelson, Jenny Barnes, Nicholas Ekins-Daukes, Benjamin Kluftinger, Ernest Tsui, and Keith Barnham, J. Appl. Phys., 82, 6240 (1997).

[43] J.P. Connolly, I.M. Ballard, K.W.J. Barnham, D.B. Bushnell, T.N.D. Tibbits, J.S. Roberts, Proc. 19th EUPVSEC, Paris, France, June 2004, pp. 355-359. Preprint: arXiv:1006.1835v2 [cond-mat.mes-hall]

[44] S. R. Kurtz, J. M. Olson, A. Kibbler, Proc. 21st lEEE PVSC, pp. 138-140 (1990).

[45] G. L. Araujo and A. Marti, Sol. Energy Mater. Sol. Cells 33, 213, 1994.

[46] I. Vurgaftman, J. R. Meyer, and L. R. Ram-Mohan, J. Appl. Phys. 89, 5815 (2001)

[47] J. C. Bourgoin, S. L. Feng, H. J. von Bardeleben, Phys. Rev. B Vol. 40, 11, pp. 7663-7670 (1989).

[48] D. J. Friedman, Sarah R. Kurtz, K. A. Bertness, A. E. Kibbler, C. Kramer, and J. M. Olson, proc. 1st WCPEC, Hawaii (1994), p. 1829.

[49] Tatsuya Takamoto, Eiji Ikeda, and Hiroshi Kurita, Masamichi Ohmori, Appl. Phys. Lett. 70 (3) (1997)

[50] Leo Esaki, IEEE Transactions on Electron Devices, vol. ed-23, no. 7, July 1976

[51] I. Garcia, et al., "A 32.6% efficient lattice-matched dual-junction solar cell working at 1000 suns," Applied Physics Letters, vol. 94, 2009, pp. 053509.

[52] R. R. King, D. C. Law, K. M. Edmondson, C. M. Fetzer, R. A. Sherif, G. S. Kinsey, D. D. Krut, H. L. Cotal, and N. H. Karam, Proc. 4th WCPEC, (2006) Hawaii, p. 760

[53] R. R. King, et al., "40% efficient metamorphic GaInP/GaInAs/Ge multijunction solar cells," Appl. Phys. Lett., vol. 90, 2007 pp. 183516-1.

[54] C. L. Andre, et al., "Impact of dislocations on minority carrier electron and hole lifetimes in GaAs grown on metamorphic SiGe substrates," Appl. Phys. Lett., vol. 84, 2004, pp. 3447.

[55] Y. Takano, et al., "Reduction of threading dislocations by InGaAs interlayer in GaAs layers grown on Si substrates, "Appl. Phys. Lett. , vol. 73, 1998 pp. 2917.

[56] S. R. Kurtz, et al., "Modeling of two-junction, series-connected tandems solar cells using top-cell thickness as an adjustable parameter," J. Appl. Phys., vol. 68, 1990, pp. 1890.

[57] W. Guter, et al., "Current-matched triple-junction solar cell reaching 41.1% conversion efficiency under concentrated sunlight," Appl. Phys. Lett., vol. 94, 2009, pp. 223504-1.

[58] N. Jain and M.K. Hudait, "Design of metamorphic dual-junction InGaP/GaAs solar cell on Si with efficiency greater than 29% using finite element analysis," in Proc. 38th IEEE Photovoltaic Spec. Conf., 2012, pp. 002056.

[59]]M. M. Wilkins, A. Boucherif, R. Beal, J.E. Haysom, J.F. Wheeldon, V. Aimez, R. Ares, T. J. Hall, and K. Hinzer, "Multijunction Solar Cell Designs Using Si Bottom Subcell and Porous Silicon Compliant Membrane, " IEEE J. Photovoltaics,vol.3, no.3, pp. 1125- 1131 , 2013.

[60] N. Jain, Y. Zhu, M. Clavel, P. Goley, M. K. Hudait, "Performance Evaluation of Monolithically Integrated 3J InGaP/GaAs/Si Tandem Solar Cells for Concentrated Photovoltaics", 40th IEEE Photovoltaic Spec Conf., Denver, CO, USA, 8-13 June, pp. 1152-1157, 2014.

[61] K. J. Schmieder, A. Gerger, M. Diaz, Z. Pulwin, M. Curtin, C.Ebert, A. Lochtefeld, R. Opila, and A. Barnett, "Progression oftandem III-V/SiGe solar cell on Si substrate, " in Proc. 27thEuropean Photovoltaic Solar Energy Coni, 2012.

[62]Nikhil Jain "Heterogeneous Integration of III-V Multijunction Solar Cells on Si Substrate: Cell Design & Modeling, Epitaxial Growth & Fabrication" Dissertation submitted to the faculty of the Virginia Polytechnic Institute and State University, 2015.

[63] N. Jain, and M.K. Hudait, "Design and Modeling of Metamorphic Dual Junction InGaP/GaAs Solar Cells on Si Substrate for Concentrated Photovoltaic Application," IEEE J. Photovoltaics, vol. 4, pp.1683-1689, 2014.

[64]. Green, M.A.; Emery, K.; Hishikawa, Y.; Warta, W. Solar cell efficiency tables (version 33). Prog. Photovoltaics Res. Appl. **2009**, 17, 85–94.

[65]Guter, W.; Schone, J.; Philipps, S.P.; Steiner, M.; Siefer, G.; Wekkeli, A.; Welser, E.; Oliva, E.; Bett, A.W.; Dimroth, F. Current-matched triple-junction solar cell reaching 41.1% conversion efficiency under concentrated sunlight. Appl. Phys. Lett. **2009**, 94, 223504.

[66] S. M. Vernon, S. P. Tobin, V. E. Haven, C. Bajgar, T. M. Dixon, M. M. Al-Jassim, et al., "Efficiency improvements in GaAs-on-Si solar cells," in Proc. 20th IEEE Photovoltaic Spec. Conf., pp. 481-485, 1988.

[67] C. L. Andre, J. A. Carlin, J. J. Boeckl, D. M. Wilt, M. A. Smith, A. J. Pitera, et al., "Investigations of high-performance GaAs solar cells grown on Ge-Si1-x-Gex-Si substrates," IEEE Trans. Electron Devices, vol. 52, pp. 1055-1060, 2005.

[68] Y. Ohmachi, Y. Kadota, Y. Watanabe, and H. Okamoto, "High Quality GaAs on Si and its Application to a Solar Cell," MRS Online Proc. Lib., vol. 144, pp. 297-302, 1988.

[69] S. M. Vernon, S. P. Tobin, V. E. Haven, L. M. Geoffroy, and M. M. Sanfacon, "High-efficiency concentrator cells from GaAs on Si," in Proc. 22nd IEEE Photovoltaic Spec. Conf., pp. 353-357, 1991.

[70] F. Dimroth, T. Roesener, S. Essig, C. Weuffen, A. Wekkeli, E. Oliva, et al., "Comparison of Direct Growth and Wafer Bonding for the Fabrication of GaInP/GaAs Dual-Junction Solar Cells on Silicon," IEEE J. Photovoltaics, vol. 4, pp. 620-625, 2014.

[71] M. R. Lueck, C. L. Andre, A. J. Pitera, M. L. Lee, E. A. Fitzgerald, and S. A. Ringel, "Dual junction GaInP/GaAs solar cells grown on metamorphic SiGe/Si substrates with high open circuit voltage,", IEEE Electron Device Lett., vol. 27, pp. 142-144, 2006.

[72] M. Diaz, L. Wang, A. Gerger, A. Lochtefeld, C. Ebert, R. Opila, et al., "Dual-Junction GaAsP/SiGe on Silicon Tandem Solar Cells," in Proc. 40th IEEE Photovoltaic Spec. Conf., 2014.

[73] K. Tanabe, K. Watanabe, and Y. Arakawa, "III-V/Si hybrid photonic devices by direct fusion bonding," Sci. Rep., vol. 2, 2012.

[74] K. Tanabe, K. Watanabe, and Y. Arakawa, "III-V/Si hybrid photonic devices by direct fusion bonding," Sci. Rep., vol. 2, 2012.

[75] J. Yang, Z. Peng, D. Cheong, and R. Kleiman, "Fabrication of High-Efficiency III-V on Silicon Multijunction Solar Cells by Direct Metal Interconnect," IEEE J. Photovoltaics, vol. 4, pp. 1149-1155, 2014.

[76] From: Innovation: Enabling a Sustainable Energy Future, by Dr. Dan E. Arvizu, 2014.

[77] J. F. Geisz, D. J. Friedman, J. S. Ward, A. Duda, W. J. Olavarria, T. E. Moriarty, et al., "40.8% efficient inverted triple-junction solar cell with two independently metamorphic junctions," Applied Physics Letters, vol. 93, p. 123505, 2008.

[78] S. D' Souza, J. Haysom, H. Anis, and K. Hinzer, "The down-to-earth future of Si substrate multijunction concentrator photovoltaic," in IEEE Electrical Power and Energy Conf., pp. 57-61, 2011.

[79] Lu ZHAO "High Efficiency Mechanically Stacked Multi-junction Solar Cells for Concentrator Photovoltaic", KatholiekeUniversiteit Leuven, 2011

[80] F. Niklaus, G. Stemme, J. Q. Lu, and R. J. Gutmann. Adhesive wafer bonding. Journal of Applied Physics, 99(3):031101, 2006.

[81] R. Songmuang et al., Photovoltaic effects in composite quantum dot structures, Proceedings of the 17th Photovoltaic European Conference (WIP-Munich and ETZ-Florence) (2001) 174.

[82] M. Ru·zinsk¶y et al., Photovoltaic and dielectric measurements on selected GaAs=AlGaAs solar cells for concentration applications, Proceedings of the 17th Photovoltaic European Conference (WIP-Munich and ETZ-Florence) (2001) 292.

[83] S. Laaksonnen et al., Gas-source molecular beam epitaxy of GaAs on Ge for solar cell applications, Proceedings of the 16th European Photovoltaic Solar Energy Conference (James & James Ltd.) (2000).

Statement of Declaration

I, the undersigned, declare that this Thesis is my original work, has not been presented for degree of Masters in any other university and that all sources of materials used for the thesis have been duly acknowledged.

NetsanetBehailu	
Name	Signature
Addis Ababa	November 2016
Place	Date

This thesis has been submitted for examination with my approval as a university advisor.

Professor Mohammed Abdo	
Advisor Name	Signature